ISSN: 2634-9221
European Journal of Applied Sciences; Vol. 14 No. 05 (2026) (01-32)
https://doi.org/10.14738/ejas.1405.12093

Impact of Weak Solar Wind Fluctuations on Ionospheric Variability in the African Equatorial Region During Geomagnetically Quiet Days at Equinox and Solstice (March and July 2014)

Jean Bienvenu Dinga[1,2], Jocelyn Franck Patient Boungou Poaty[1,2,3], Brice Rodrigue Malonda Boungou[1,3], Jean Louis Zerbo[4]

1. Université Marien NGOUABI, Brazzaville, République du Congo
2. Laboratoire de Physique de l'Atmosphère de l'Institut National de Recherche en Sciences Exactes et Naturelles, République du Congo
3. Université Denis SASSOU N'GUESSO, République du Congo
4. Université Nazi BONI Bobo-Dioulasso, Burkina Faso

Abstract: This study "Impact of weak solar wind fluctuations on ionospheric variability in the African equatorial region during geomagnetically quiet days at equinox and solstice (March and July 2014)", analyses the variability of the ionospheric Total Electron Content (TEC) in the African equatorial region, focusing on the impact of minor solar wind fluctuations during geomagnetically quiet periods. Based on GNSS data from four stations (ADIS, BJCO, MBAR, NKLG) for equinox (March 2014) and solstice (July 2014) periods, the analysis systematically compares TEC variations with solar and geomagnetic parameters. The results confirm marked diurnal and seasonal variability, with significantly higher TEC in March (80–105 TECU) than in July (40–60 TECU). The major contribution of the study lies in the distinction between diurnal and nocturnal correlation regimes. During the night (19:00–24:00 UT), in the absence of photo-ionization, very strong and statistically significant correlations (coefficients often exceeding 0.8) are observed between TEC and solar wind speed ($\boldsymbol{V_x}$), the ($\boldsymbol{B_z}$) component of the interplanetary magnetic field, and the $\boldsymbol{SYM\_H}$ index. During the day, TEC variability is primarily linked to solar radiation, with solar wind temperature being the most correlated parameter. This study demonstrates that even subtle solar perturbations significantly modulate the African equatorial ionosphere, particularly at night, highlighting the importance of a multi-parameter approach for precise modeling in this region.

Keywords: Total Electron Content (TEC), Equatorial Ionosphere, Solar Wind, Geomagnetically Quiet Periods, Ionosphere-Sun Correlation.

INTRODUCTION

It is clearly established that the ionosphere plays an important role in understanding space weather and radio signal transmission, which are central to any tool using electromagnetic signals such as navigation and telecommunications. Total Electron Content (TEC), calculated from GNSS data, is a valuable parameter for monitoring variations in ionospheric activity. At the magnetic equator, the ionosphere is subject to a phenomenon called the Equatorial Ionization Anomaly (EIA), which alters the normal distribution of ionospheric electron density. These variations can disrupt the proper functioning of satellites, making the study of TEC a topical subject for both science and daily applications.

However, the African equatorial region remains under-exploited due to a lack of continuous GNSS data and insufficient station coverage, making every analysis of this zone unique. Previous research has primarily studied perturbations caused by geomagnetic storms. For instance, Data (2025) [1] showed that a super-storm in May 2024 led to significant positive and negative TEC anomalies in South Africa. Similarly, Ram and al. (2024) [2] highlighted global TEC increases exceeding 100% over the EIA, accompanied by poleward shifts of crests caused by prompt penetration electric fields (PPEF).

Although these studies provide valuable insight into extreme geomagnetic events, much remains to be learned about more subtle TEC fluctuations during quiet periods when geomagnetic activity is low. low. **Joshua and al. (2021) [3]** and **Koala and al. [4]** showed that even small variations in solar wind can have a significant impact on the behavior of the low-latitude ionosphere during quiet periods. They emphasize the importance of analyzing multiple parameters simultaneously to better understand these phenomena.

In the African equatorial region, **Falayi and al. (2023) [5]** used wavelet power spectrum analysis to study TEC during quiet periods of solar cycle 24. Their study shows that factors such as $\vec{E} \times \vec{B}$ drifts, thermospheric composition (O/N_2), and meridional winds play a key role in these variations, while dynamics near the magnetic equator remain generally more stable than at higher latitudes.

Our work, based on quiet periods, complements research that focuses primarily on storms. It also provides a better understanding of how several solar parameters-such as the Interplanetary Magnetic Field (IMF), the interplanetary electric field, solar wind properties, and the geomagnetic index Dst or SYM_H, interact to induce subtle changes in TEC in a region where few instruments are installed.

In this study, we analyzed GNSS data collected from four stations located in Ethiopia (ADIS), Benin (BJCO), Uganda (MBAR), and Gabon (NKLG). The objective was to study how Total Electron Content (TEC) varies on a day-to-day and monthly basis. To strictly ensure the reliability of the results, only days where geomagnetic activity was quiet were taken into account, specifically those in March and July 2014. This avoids variations due to storms or perturbations skewing the analysis. Then, all these TEC variations were systematically compared to solar and geomagnetic parameters to better understand which factors most influence these changes during a period without intense geomagnetic activity.

This work is among the few studies exploring how multiple solar parameters act together on TEC during quiet periods in the African equatorial region. While most previous research has focused on solar storms or correlations involving one or two parameters, this study highlights the fine interactions between the Sun and the ionosphere in a zone where few instruments are available. The comparison between equinox and solstice periods brings new information on how the season influences the Sun-Earth relationship, which helps refine regional ionospheric models.

The main objectives of this study are, first, to better understand how TEC varies throughout the day and according to seasons. Second, it aims to identify which solar and geomagnetic parameters are most linked to these variations. The third step consists of distinguishing TEC changes caused by solar activity from those primarily influenced by insolation. Finally, this study aims to provide a reference dataset that can help model the ionosphere in regions where data is scarce.

This study is structured into five parts: the first presents the datasets and methods used to derive and process TEC as well as solar parameters. The second describes the criteria for selecting quiet days and provides an overview of the analyzed stations and their geographic distribution. The third presents the results, including the diurnal and seasonal variability of TEC and its correlations with the considered parameters. The fourth discusses the implications of these results within the framework of ionospheric modeling and space weather studies in Africa. Finally, the fifth summarizes the main conclusions and proposes perspectives for future research.

DATASETS AND METHODOLOGY FOR TEC AND SOLAR PARAMETER ANALYSIS

This study, titled "Impact of weak solar wind fluctuations on ionospheric variability in the African equatorial region during geomagnetically quiet days at equinox and solstice (March and July 2014)," examines the influence of minor solar wind variations on Total Electron Content (TEC) during geomagnetically quiet days.

Data Sources

To carry out this work, we used a dataset ensuring effective analysis of TEC and solar parameters, namely:

- **RINEX Files:** Dual-frequency GPS observations providing local daily TEC **[6]**.
- **CODG Files (IONEX):** Providing Global daily TEC, data supplied by CODE **[7]**.
- **DCB Files:** Used to correct monthly differential code biases of satellite and receiver clock offsets **[7].**
- **YUMA Files (Almanacs):** Ephemeris files, calculating the precise position of satellites at any instant (weekly) **[8].**
- **Magnetic and Solar Wind Parameters:** Interplanetary magnetic field $\boldsymbol{B_z}$, interplanetary electric field $\boldsymbol{E_y}$, solar wind speed $\boldsymbol{V_x}$, density $\boldsymbol{D}$, temperature $\boldsymbol{T}$, pressure $\boldsymbol{P}$, and the geomagnetic index $\boldsymbol{SYM\_H}$ (characterizing $\boldsymbol{Dst}$), provided by OMNIWeb every 5 minutes **[9].**

The combination of these high-resolution multi-source data constitutes one of the central elements of the originality of our study, enabling the examination of subtle Sun-ionosphere interactions in a sparsely covered region.

TEC Calculation

The pseudorange $P_i^s(f)$ between receiver r and satellite s at frequency f is given by:

$$P_i^s(f) = \rho_r^s + c \cdot [b_i(f) - b^s(f)] + T_{trop} + I_i + \alpha_j^i(f)$$

Where:

- ρ_r^s is the geometric distance,
- $b_i(f), b^s(f)$ are the receiver/satellite clock errors,

- T_{trop} is the tropospheric delay,
- I_i is the ionospheric delay,
- $\alpha_j^i(f)$ groups measurement and multipath errors.

From dual-frequency measurements Warnant, 1996 **[10]**, the ionospheric delay is isolated, and the **Slant TEC (STEC) [11],[12]** is calculated:

$$STEC = \frac{f_1^2 \cdot f_2^2}{40.3 \cdot (f_1^2 - f_2^2)} \left(P_{L_1} - P_{L_2}\right)$$

Then, the **Vertical TEC (VTEC)** is obtained using the Single Layer Model (SLM):

$$TEC = STEC \sqrt{1 - \left(\frac{R_E}{R_E + H_{PI}} cos\beta\right)^2}$$

Where:

- R_E: Earth radius
- H_{PI}: Height of the ionospheric layer
- H_{PI}: Satellite elevation angle

Processing Chain and MATLAB Scripts

File Processing by MATLAB Scripts Yielding Daily, Monthly, and Annual VTEC

The script (***tec_notigs.m***), developed by Rolland Fleury **[13]**, was used to automate the processing of daily RINEX files (format 2.x). The processing flow checks file integrity, decompresses supported formats, and removes obsolete files. The main steps are:

- Automatic download of necessary files (RINEX, CODG, DCB, and YUMA).
- Calculation of STEC from pseudorange differences.
- Conversion of STEC to VTEC via the ionospheric projection function.
- Validation of VTEC by comparison with CODG data, accompanied by the generation of a comparative figure (RINEX VTEC vs. CODG).
- Production of a text file for each processed day containing CODG values and smoothed VTEC values (every 15 minutes).

The script (***vtec_time_1_month.m***), developed by Rolland Fleury **[13]**, uses the smoothed VTEC values from the text files generated by (tec_notigs.m) to produce a continuous monthly representation of VTEC. The main steps are:

- Reading the daily smoothed VTEC text files generated by (tec_notigs.m).
- Chronological organization and concatenation of data over the entire month.
- Generation of a monthly VTEC time series (15-minute time step).
- Visualization of monthly curves for better analysis of intra-monthly variability.

The script (***tec_2d_tl.m***), developed by Rolland Fleury, was used to generate an annual representation of vertical total electron content (VTEC) as a function of the day of the year and local time for a given GNSS station in the form of a 2D Map for global visualization.

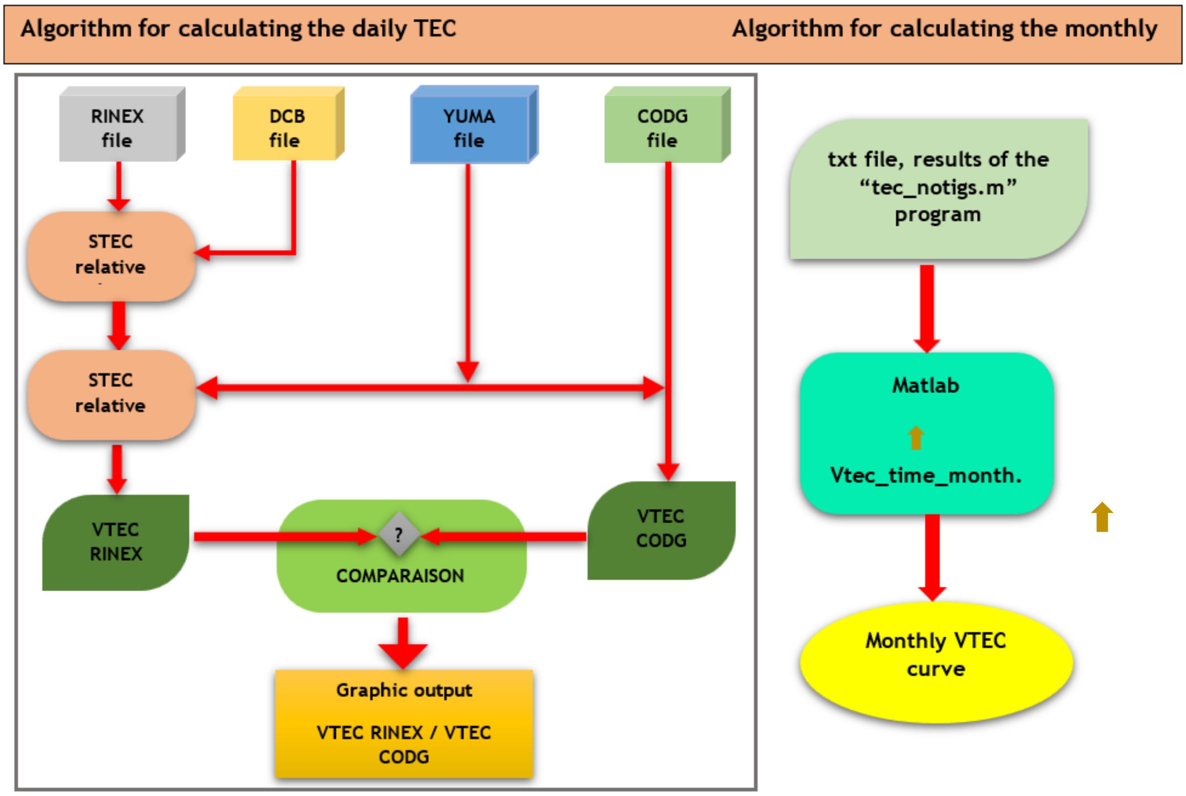

Figure 1: Algorithms for Computing Daily and Monthly TEC

File Processing by MATLAB Scripts Yielding Solar Parameters and Correlations between VTEC and Solar Parameters

The script (***solar_data_plot.m***) was used to analyze and graphically represent solar parameters on daily periods. The main steps are:

- Reading files containing solar and geomagnetic parameters V_x, B_z, E_y, D, T, P, Dst, $or\ SYM\_H$, etc.).
- Automatic correction of outliers using predefined thresholds for each parameter.
- Organization of data by day and generation of multi-parameter figures.

The script (***VTEC_Cor_Solarwind.m***) was used to analyze the relationship between VTEC and solar parameters. It allows for a quantitative evaluation of the influence of solar wind fluctuations on ionospheric variability. The main steps are:

- Reading the daily smoothed VTEC text files generated by the script (***tec_notigs.m***).
- Loading solar and interplanetary parameters.
- Interpolation of VTEC and solar series to ensure comparability.

- Calculation of Pearson, Spearman, and Kendall correlation coefficients (r) between VTEC and each selected solar parameter for a full day and for the night (19:00–24:00 UT).
- Estimation of statistical significance through p-values ($p < 0.05$).
- Graphic visualization of relationships (superimposed time series, scatter plots).
- Production of figures and reports summarizing correlation coefficients.

CHOICE OF STATIONS, PERIOD, AND DATA USED

The selected GPS stations: **Adis (Ethiopia), Bjco (Benin), Mbar (Uganda), and Nklg (Gabon)** cover different longitudinal sectors of the African magnetic equatorial band. They were chosen based on two main criteria: the simultaneous availability of complete RINEX files for all considered days, and geographic representativeness within the low-latitude ionospheric region to ensure broad spatial coverage.

The study periods chosen were March and July 2014, corresponding respectively to the **equinox** and **solstice**, as visualized by annual TEC, to examine diurnal and seasonal TEC variability under representative conditions. To ensure a relevant statistical basis, all geomagnetically quiet days (Q-days) in these two months with available data were selected.

Tableau 1: Geographical Coordinates of the Selected Stations

Country	Station	Latitude	Longitude
Ethiopia	Adis	9.035°N	38.766°E
Benin	Bjco	6.385°N	2.450°W
Uganda	Mbar	0.601°S	30.7374°E
Gabon	Nklg	0.354°N	0.672°E

Table 1 shows that regarding latitude, only the MBAR station is in the southern hemisphere. Furthermore, all stations are east of the Greenwich meridian except for the BJCO station.

The selected quiet days are ranked from calmest to moderate as follows **[14]**:

- **March:** 16, 9, 17, 7, 8, 11, 24, 10, 15, 19.
- **July:** 19, 18, 20, 1, 29, 6, 5, 17, 30, 16.

RESULTS

Diurnal Variability of TEC During Quiet Days

Analysis of annual VTEC curves (**Figure 2a,b**) reveals two distinct regimes: high values between February–May and September-December, and low values between June-August. This trend is observed homogeneously across all four stations, leading to the selection of March and July for this study.

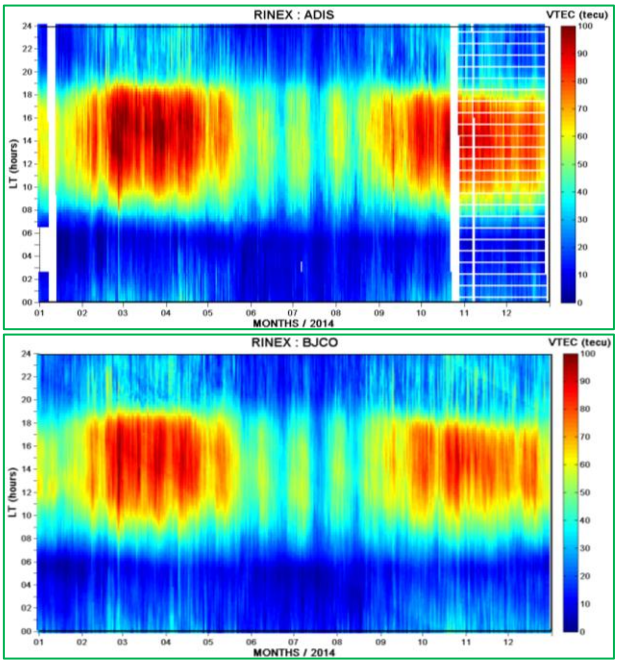

Figure 2a: Annual Variation of TEC from Text Files Derived from RINEX Data for the Stations (ADIS and BJCO).

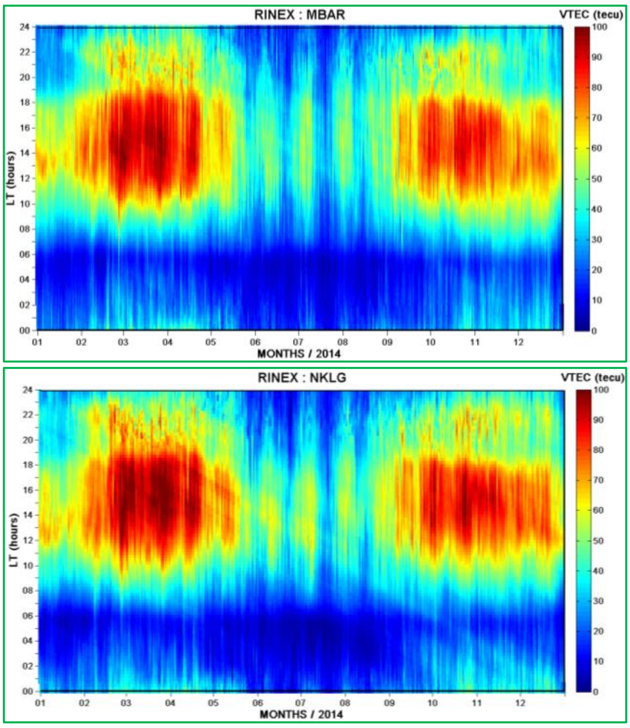

Figure 2b: Annual Variation of TEC from Text Files Derived from RINEX Data for the Stations (MBAR, and NKLG).

Monthly variations confirm marked seasonal variability: March corresponds to a period of **high TEC** (80–105 TECU), while July reflects a period of **low TEC** (25–60 TECU), a trend confirmed across all stations.

The analysis of data from the four GNSS stations shows that the daily variability of TEC follows a characteristic pattern of the equatorial region (**Figure 4, Figure 5, and Appendix 1**).

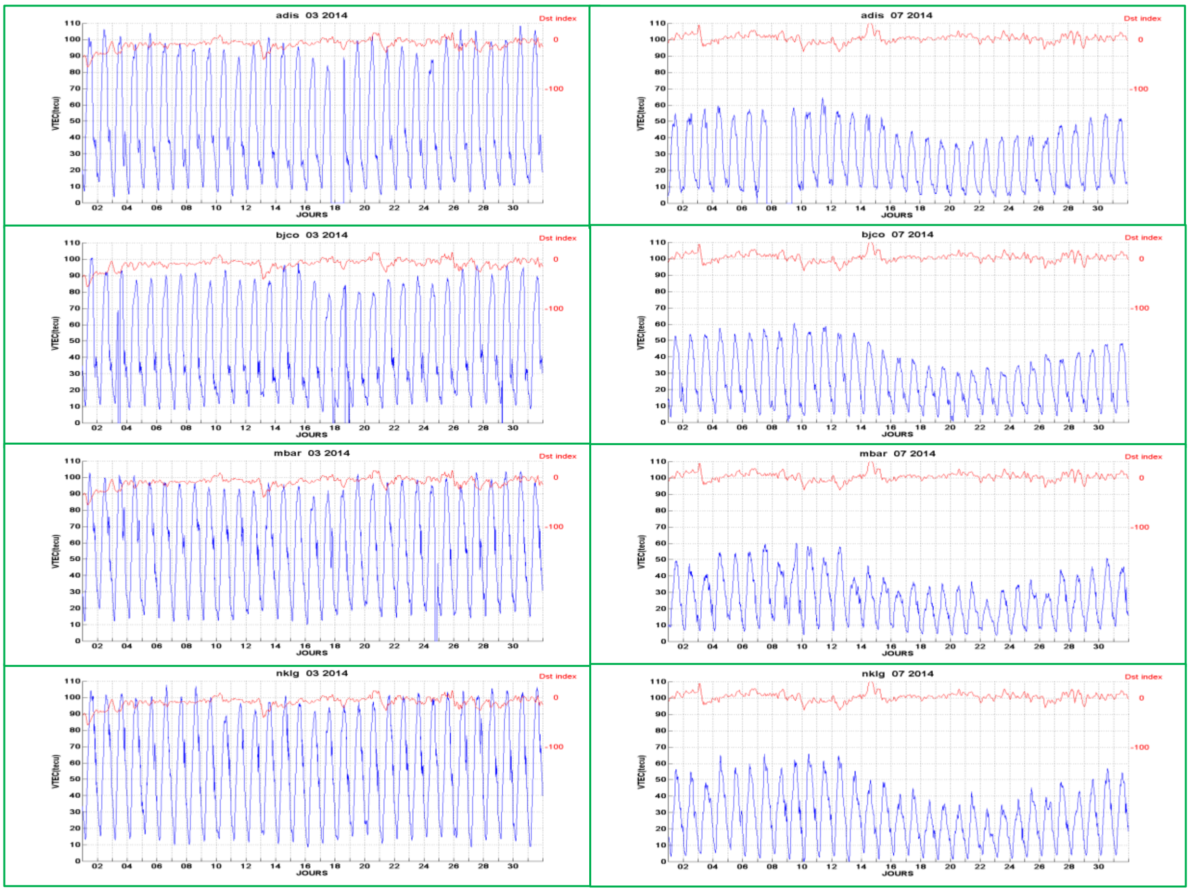

<u>Figure 3</u>: Monthly variation of TEC for the months of march (left) and July (right) 2014 from text files derived from RINEX data for the stations (ADIS, BJCO, MBAR, and NKLG).

In our study, we do not focus on these discrepancies but rather on the contribution of solar wind parameters to the daily variations observed in the TEC curves derived from the RINEX data. Regarding the daily variability of TEC:

We generally observe, regardless of the season or the station:

- a progressive increase in TEC after sunrise between 5:00 and 6:00 UT, with a pronounced maximum around midday between 12:00 and 16:00 UT,
- followed by a gradual decrease toward nighttime hours.
- This diurnal evolution reflects the dynamics of photo-ionization, which is strongly linked to solar radiation.
- The maximum amplitudes vary from one station to another, reflecting the influence of longitude and proximity to the magnetic equator. For example, the NKLG station (Gabon) generally shows higher VTEC values than the other stations, indicating a marked longitudinal variability.

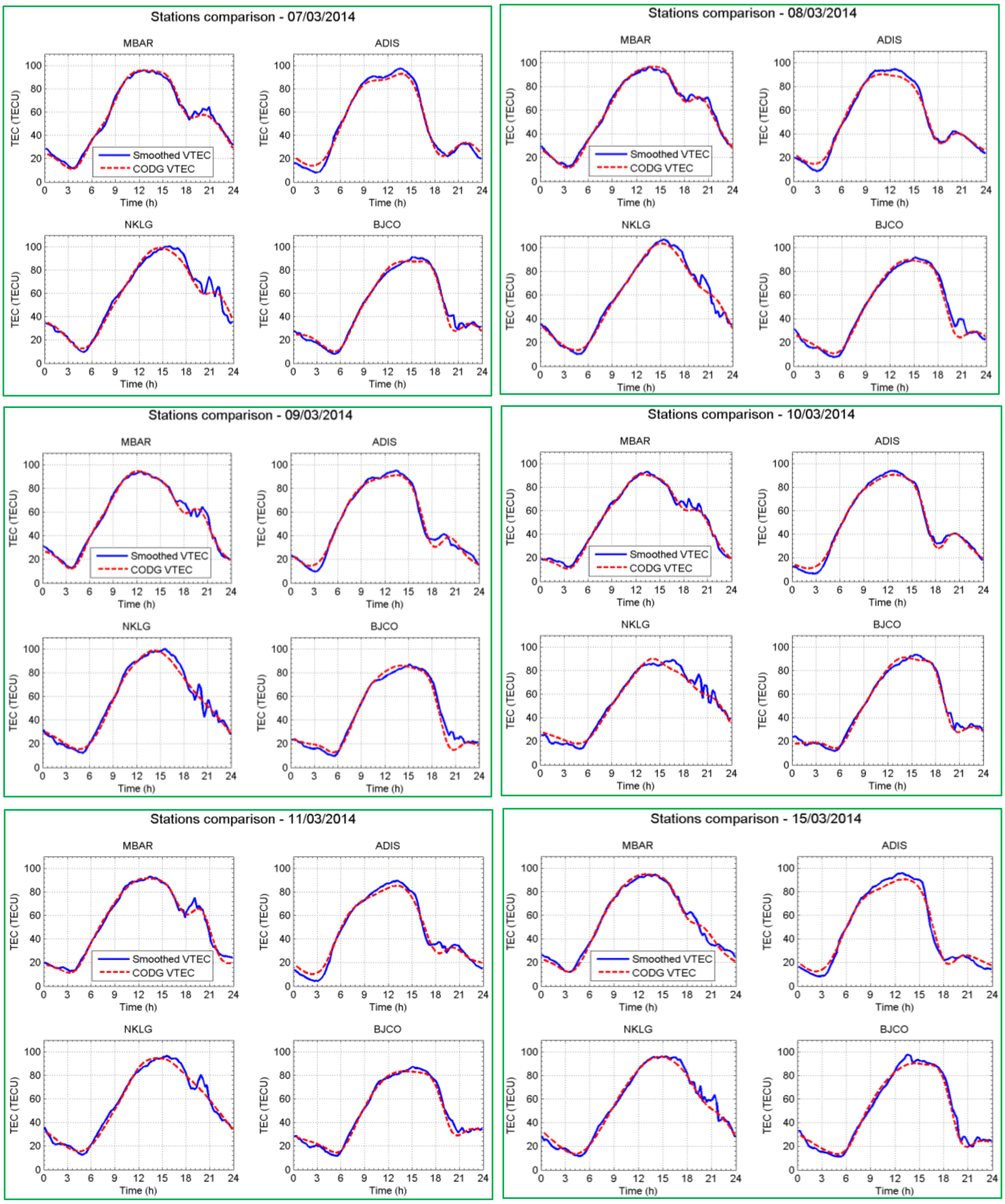

Figure 4: Diurnal variability of VTEC on quiet days in March 2014 for the four stations (ADIS, BJCO, MBAR, and NKLG)

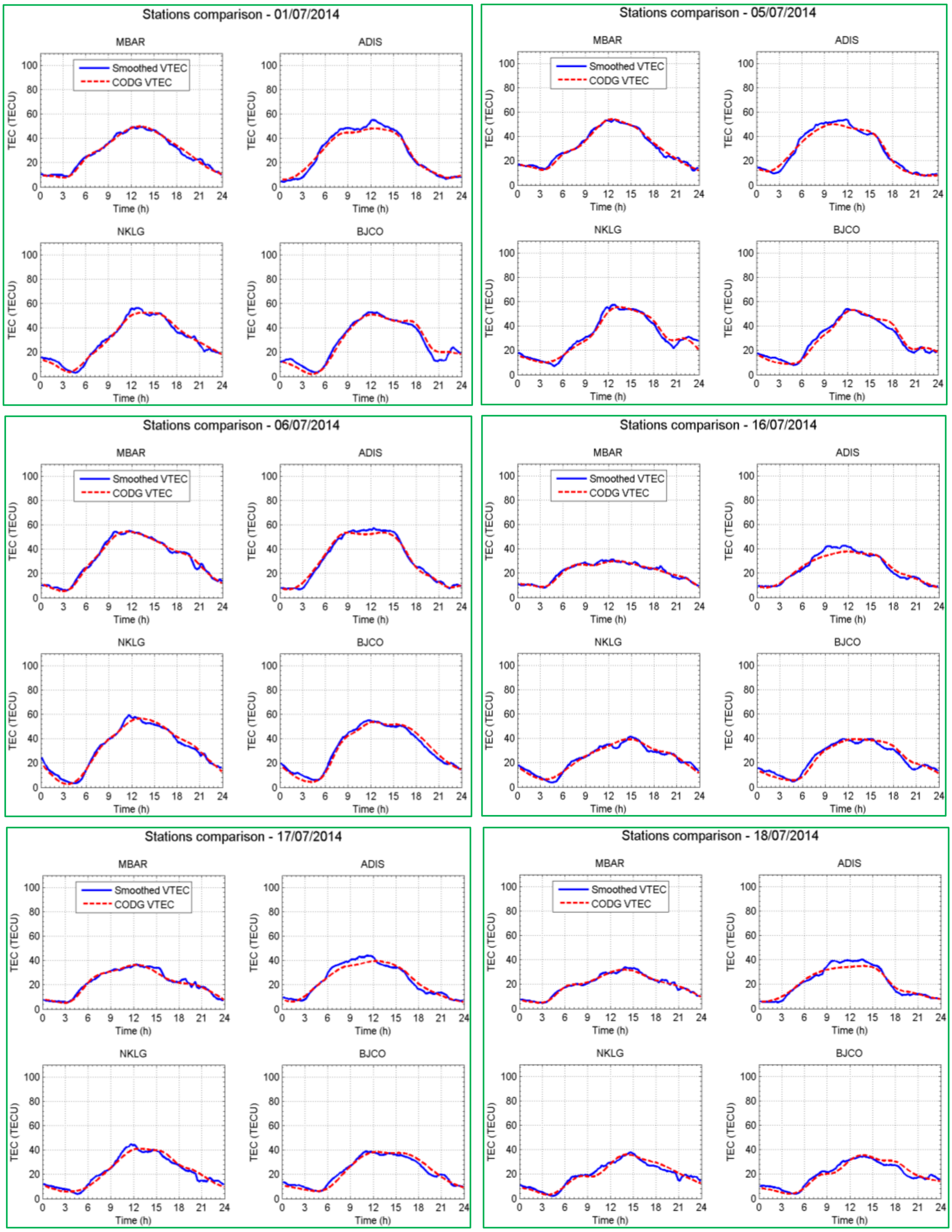

Figure 5: Diurnal variability of VTEC on quiet days in July 2014 for the four stations (ADIS, BJCO, MBAR, and NKLG)

Seasonal Variability: Equinox-Solstice Comparison

The comparison between March (equinox) and July (solstice) 2014 highlights notable differences:

- In **March**, diurnal TEC maxima are more intense (80–110 TECU), reflecting ionization enhanced by equinox conditions.
- In **July**, TEC shows lower average values (40–60 TECU), with a broader crest of maxima between 10:00 and 18:00 UT.

These results confirm that the season plays an important role in modulating TEC, interacting with $\vec{E} \times \vec{B}$ drift dynamics and variations in solar inclination.

Inter-Station Comparison

Joint examination of the four stations shows an influence linked to their geographic position on TEC variability:

- For March:
  - NKLG (Gabon): Located near the equator, it presents the highest maxima, reflecting the particular intensity of the Equatorial Ionization Anomaly (EIA) in this sector.
  - ADIS (Ethiopia) and MBAR (Uganda): Located north-east and south-east of the equator respectively, they show relatively close TEC amplitudes, demonstrating a certain interhemispheric symmetry given that the magnetic equator differs from the geographic equator.
  - BJCO (Benin): The only station west of the Greenwich meridian, it records slightly lower values and a temporal shift in maxima, a direct consequence of its specific longitudinal position.
- For July: Differences are barely noticeable as all stations show nearly identical maxima. The differences observed, especially in March, confirm that magnetic latitude and longitude play a determining role in regional TEC dynamics.

Impact of Subtle Solar Fluctuations on TEC in Quiet Conditions

Analysis of solar parameter curves Analysis of solar parameter curves (V_x, B_z, E_y, D, T, P, Dst, $or\ SYM\_H$) **Figures 6-a to 7-b and Appendix 2** reveals significant nuances between the days of March and July 2014.

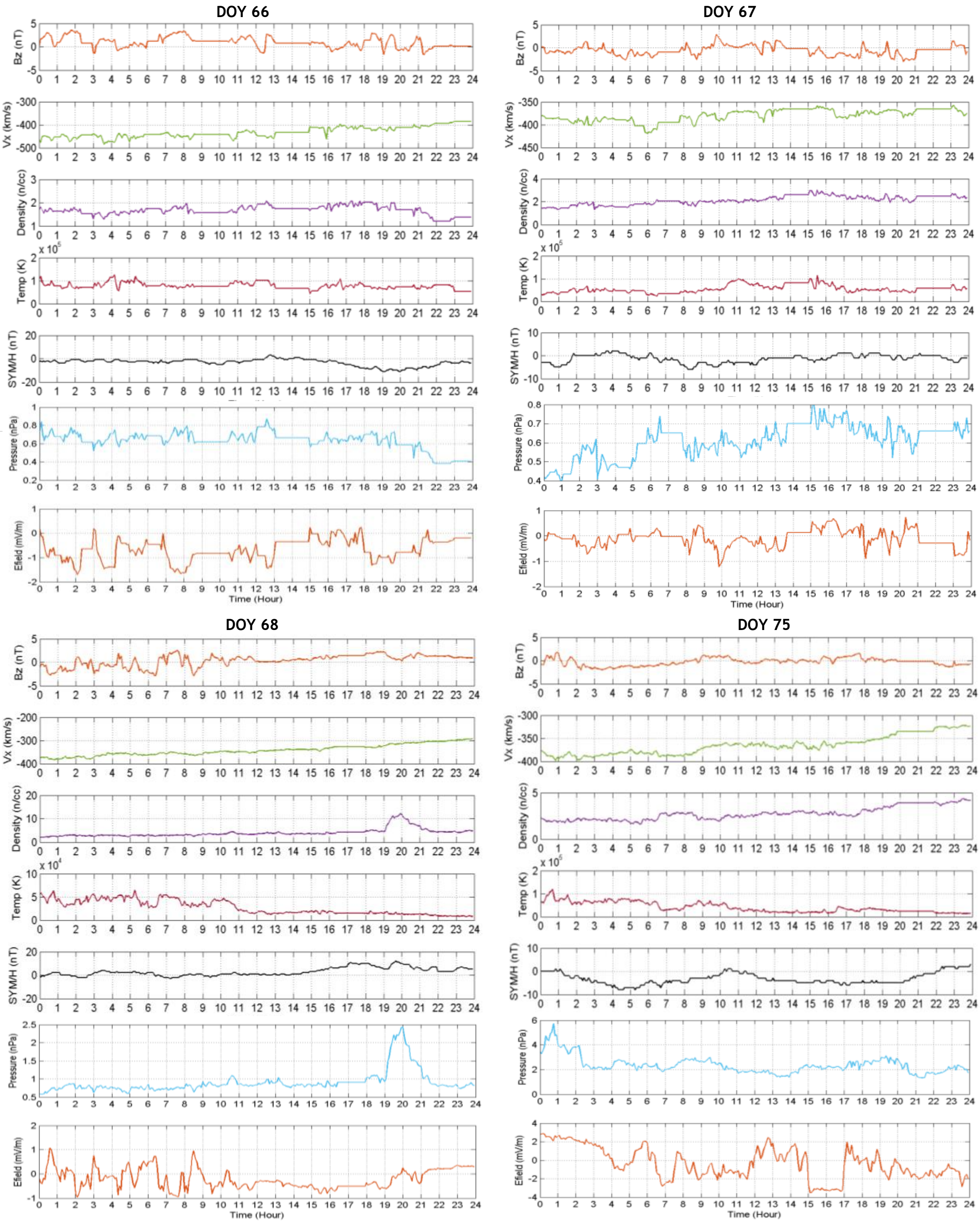

<u>Figure 6 a</u>: Evolution of Solar Wind Parameters (V_x, B_z, E_y, D, P, T, and SYM-H) during quiet days in March 2014 (7, 8, 9, 16)

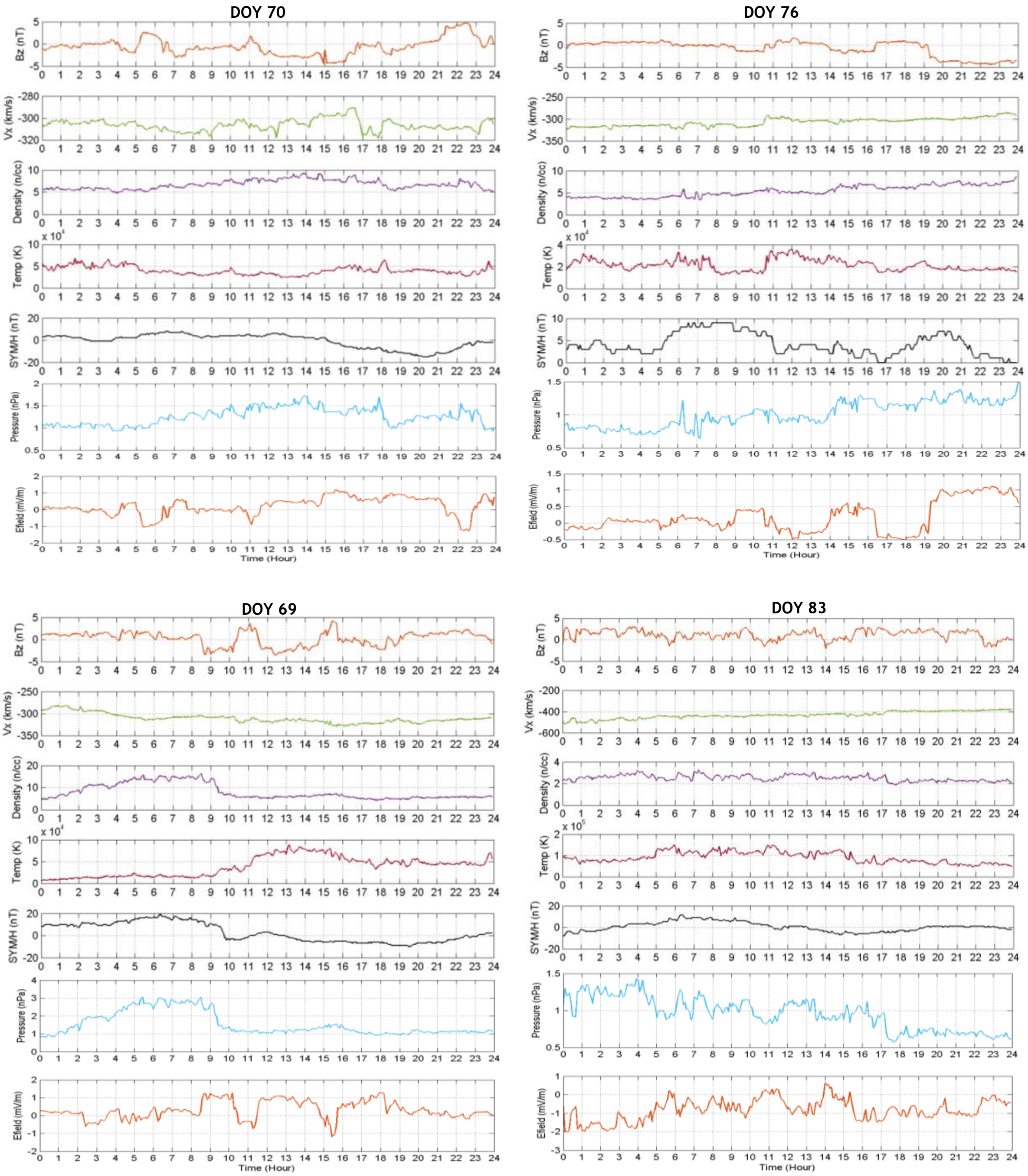

Figure 6 b: Evolution of solar wind parameters (V_x, B_z, E_y, D, P, T, and SYM-H) during quiet days in March 2014 (10, 11, 17, 24)

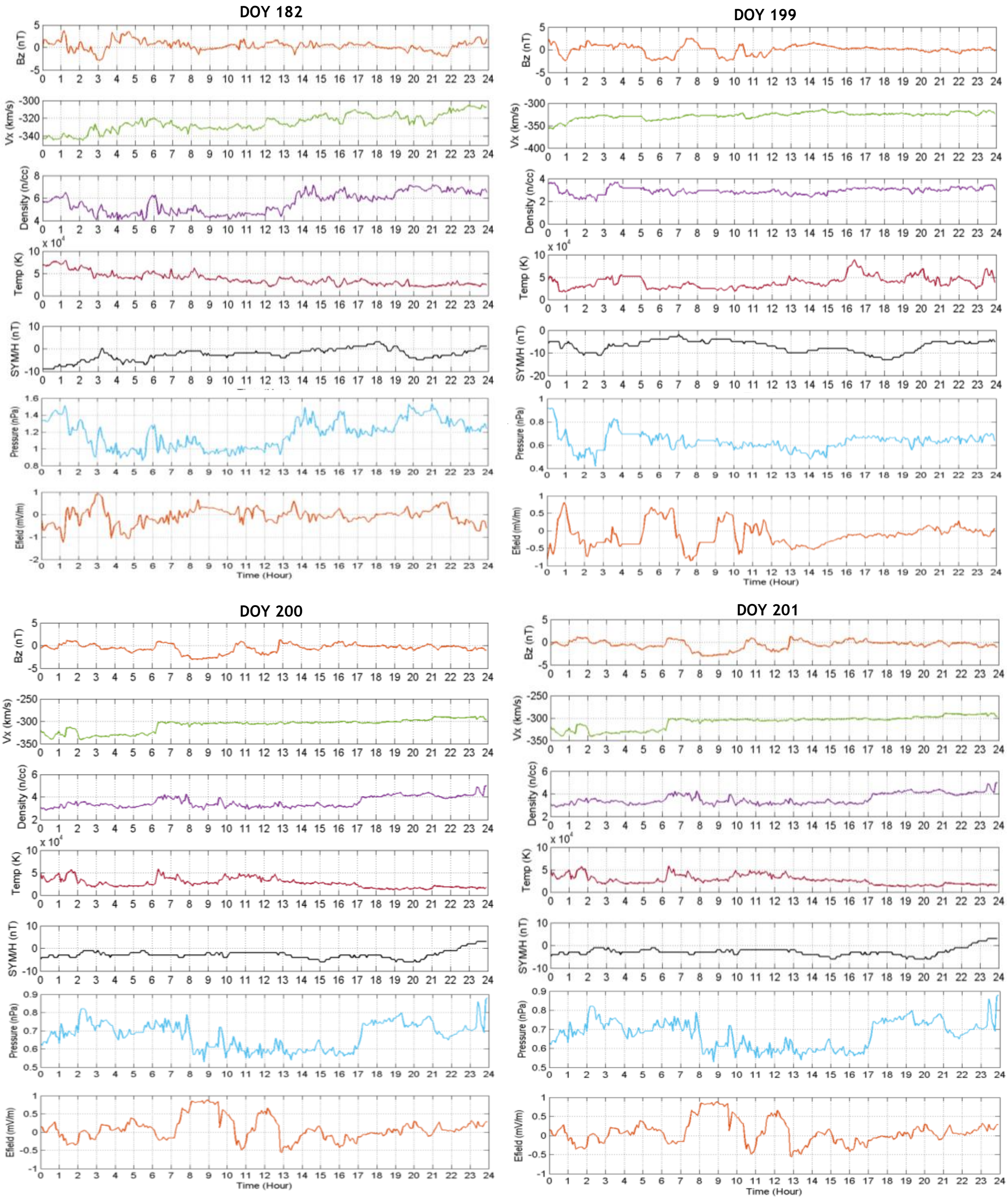

Figure 7 a: Evolution of solar wind parameters (V_x, B_z, E_y, D, P, T, and SYM-H) during quiet days in July 2014 (1, 18, 19, 20).

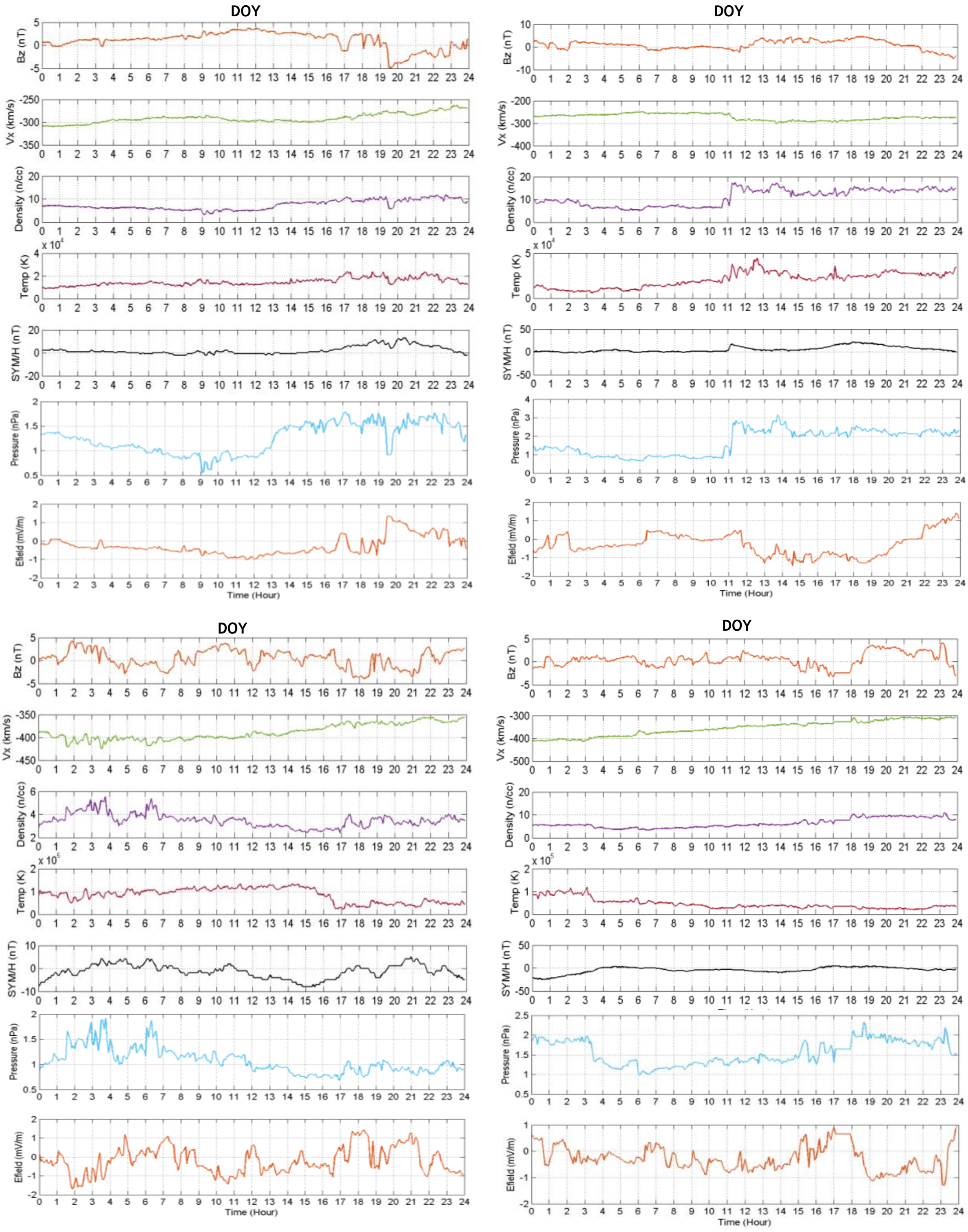

<u>Figure 7 b</u>: Evolution of Solar Wind Parameters (V_x, B_z, E_y, D, P, T, and SYM-H) During Quiet Days in July 2014 (5, 6, 17, 29).

Tableau 2: Hourly summary of the ionospheric parameters (NKLG) and solar wind parameters for the geomagnetically quiet days of March 2014 (7, 8, 9, 10, 11, 15, 16, 17, 19, 24)

Day	Intervale	TEC (tecu) Nklg	Speed (km/s)	Pressure (nPa)	Bz (nT)	Efield (mV/m)	Density (p/cc)	Temperature (K)	SYM/H (nT)
7 March	00h-08h	9.76-42.43	-484.40 to -433.80	0.52-0.84	-1.39 to 3.52	-1.70 to 0.21	1.30-1.86	55985-125992	-4 to -1
	08h-16h	45.43-100.51	-471.70 to -408.20	0.56-0.87	-1.39 to 3.36	-1.63 to 0.24	1.53-2.08	44563-102332	-5 to 3
	16h-24h	34.26-99.28	-431.60 to -385.60	0.38-0.74	-1.62 to 2.89	-1.31 to 0.25	1.21-2.07	54057-108482	-11 to -1
8 March	00h-08h	10.11-43.71	-418.70 to -379.10	0.40-0.74	-2.63 to 1.33	-0.73 to 0.31	1.33-2.17	22791-66645	-5 to 2
	08h-16h	46.40-106.82	-404.00 to -358.90	0.50-0.80	-2.55 to 2.84	-1.22 to 0.57	1.59-3.03	34837-113850	-6 to 0
	16h-24h	34.93-102.93	-387.40 to -357.70	0.52-0.77	-3.05 to 1.43	-0.89 to 0.73	1.90-2.81	37624-86262	-3 to 1
9 March	00h-08h	12.05-43.72	-383.10 to -348.90	0.58-0.87	-2.87 to 2.55	-0.96 to 1.07	2.05-3.27	26403-64511	-3 to 4
	08h-16h	47.31-100.07	-364.70 à -333.30	0.64-1.09	-2.87 to 1.94	-0.82 to 0.95	2.43-4.44	12315-47080	-2 to 5
	16h-24h	28.06-97.02	-331.80 to -290.80	0.74-2.43	0.26 to 2.24	-0.72 to 0.36	3.64-12.12	7357-19908	3 to 12
10 March	00h-08h	13.67-41.51	-315.60 to -281.90	0.81-3.06	-0.24 to 2.34	-0.62 to 0.45	4.73-15.64	7160-23422	7 to 19
	08h-16h	44.23-88.12	-329.80 to -304.80	1.03-3.05	-3.60 to 4.05	-1.18 to 1.27	4.96-16.28	12483-88132	-6 to 14
	16h-24h	38.27-89.06	-329.10 to -308.40	0.91-1.37	-2.25 to 2.21	-0.20 to 1.26	4.35-6.42	32032-70105	-10 to 2
11 March	00h-08h	12.50-42.35	-314.80 to -300.50	0.92-1.34	-3.09 to 2.54	-1.04 to 0.64	4.84-6.83	28844-67893	-1 to 8
	08h-16h	45.16-96.58	-317.90 to -295.60	1.19-1.73	-4.37 to 1.81	-0.89 to 1.19	6.21-9.27	23384-49339	-5 to 6
	16h-24h	34.42-94.53	-318.60 to -290.70	0.93-1.70	-4.07 to 4.67	-1.29 to 1.08	5.12-8.92	26757-64298	-15 to -1
15 March	00h-08h	11.63-44.17	-415.60 to -392.90	0.69-1.02	-3.03 to 1.67	-0.89 to 0.95	2.10-3.16	43596-129592	-14 to -4
	08h-16h	46.78-96.32	-423.00 to -382.30	0.57-0.87	-0.05 to 3.31	-1.35 to 0.28	1.83-2.85	44760-107347	-6 to 1
	16h-24h	28.21-95.39	-412.60 to -377.00	0.50-0.93	-2.31 to 1.40	-0.73 to 0.69	1.61-3.25	40867-143034	-10 to 2
16 March	00h-08h	8.58-41.27	-398.50 to -374.60	0.47-0.87	-2.06 to 1.77	-1.06 to 0.60	1.62-2.91	25571-119428	-8 to 1
	08h-16h	44.39-91.10	-386.00 to -354.90	0.52-0.86	-0.68 to 1.20	-0.55 to 0.23	1.94-3.07	16165-69458	-5 to 1
	16h-24h	32.13-91.80	-370.90 to -321.90	0.62-0.91	-1.34 to 1.54	-0.65 to 0.01	2.42-4.38	12843-44360	-6 to 3
17 March	00h-08h	10.96-46.68	-324.40 to -307.10	0.64-1.22	-0.82 to 1.17	-0.23 to 0.26	3.34-5.89	15511-33289	2 to 9
	08h-16h	49.23-93.91	-320.00 to -290.10	0.83-1.30	-1.92 to 1.62	-0.47 to 0.62	4.25-7.22	12214-35883	1 to 9
	16h-24h	28.62-91.76	-305.80 to -285.70	1.05-1.50	-4.35 to 0.93	-0.50 to 1.11	5.74-8.62	14718-25177	0 to 7
19 March	00h-08h	15.21-47.12	-332.70 to -300.90	1.28-2.12	-3.33 to 6.31	-1.42 to 1.48	6.79-10.32	36850-99706	-5 to 3
	08h-16h	48.64-96.93	-316.50 to -297.10	1.17-1.38	-3.71 to 2.96	-1.27 to 1.26	6.10-7.46	54559-128743	-8 to 3
	16h-24h	31.02-93.04	-320.60 to -289.90	0.97-1.37	-3.21 to 3.34	-0.54 to 1.23	5.35-7.31	32873-78539	-3 to 7
24 March	00h-08h	14.71-43.24	-516.10 to -435.70	0.87-1.43	-1.47 to 2.95	-2.03 to 0.23	2.09-3.26	58578-149309	-8 to 11
	08h-16h	44.87-99.03	-460.50 to -418.80	0.81-1.16	-2.08 to 2.84	-1.45 to 0.66	2.17-3.04	61763-148996	-7 to 9
	16h-24h	33.06-98.69	-432.90 to -379.80	0.57-1.12	-1.71 to 2.82	-1.47 to -0.02	1.88-3.03	45082-100016	-6 to 1

- **In March:** Solar wind parameters, particularly speed (V_x) and temperature (T), are quite high, with lower densities (D). The interplanetary magnetic field (B_z) and the SYM-H index display significant variability throughout the days, oscillating between positive and negative values. This indicates variable geomagnetic activity even during "quiet" periods.

- **In July:** Solar wind density reaches higher values, and the SYM_H index presents more negative values. Wind speed and temperature are moderate, distinguishing the winter-spring equinox from the summer solstice. The SYM_H index suggests that, despite being classified as "quiet days," geomagnetic conditions in July were more perturbed than in March on certain days.

This differentiation forms the basis for correlation analysis, suggesting that the ionospheric response is not uniform and depends on specific solar wind conditions.

Tableau 3: Hourly summary of the ionospheric parameters (NKLG) and solar wind parameters for the geomagnetically quiet days of July 2014 (1, 5, 6, 16, 17, 18, 19, 20, 29, 30).

Day	Intervale	TEC (tecu) Nklg	Speed (km/s)	Pressure (nPa)	Bz (nT)	Efield (mV/m)	Density (p/cc)	Temperature (K)	SYM/H (nT)
1 July	00h-08h	3.27-25.55	-344.60 to -319.20	0.86-1.51	-2.83 to 3.68	-1.23 to 0.91	4.06-6.49	35314-79261	-9 to 0
	08h-16h	28.44-56.24	-333.60 to -314.30	0.91-1.49	-1.66 to 1.91	-0.46 to 0.66	4.12-7.16	19299-62381	-4 to 0
	16h-24h	18.49-50.03	-328.60 to -304.90	1.13-1.53	-2.00 to 2.28	-0.73 to 0.56	5.64-7.19	19558-39363	-5 to 3
5 July	00h-08h	7.15-27.45	-309.70 to -287.80	0.83-1.38	-0.29 to 2.11	-0.60 to 0.11	4.88-7.21	8906-15233	-2 to 3
	08h-16h	27.32-57.40	-300.30 to -284.70	0.55-1.63	1.19 to 3.67	-1.02 to -0.25	3.25-9.12	11619-17954	-2 to 2
	16h-24h	21.62-51.97	-295.40 to -262.80	0.91-1.79	-4.89 to 2.63	-0.77 to 1.36	5.79-11.66	12453-23926	-2 to 13
6 July	00h-08h	3.36-34.67	-271.40 to -247.80	0.66-1.49	-1.62 to 2.74	-0.75 to 0.46	5.12-10.19	6165-15372	-2 to 5
	08h-16h	35.06-59.71	-301.70 to -252.50	0.78-3.16	-2.26 to 4.47	-1.44 to 0.47	6.07-17.36	14412-44546	-1 to 17
	16h-24h	16.17-48.79	-296.40 to -272.50	1.92-2.58	-5.01 to 4.51	-1.30 to 1.41	11.38-15.81	18705-35754	0 to 21
16 July	00h-08h	3.77-22.79	-469.90 to -388.30	0.57-1.30	-3.05 to 2.72	-1.38 to 1.03	1.85-3.12	36197-108303	-14 to 2
	08h-16h	23.73-41.33	-424.00 to -384.80	0.51-1.05	-3.25 to 2.00	-1.16 to 0.70	1.57-3.06	36606-146476	-12 to -3
	16h-24h	13.34-37.43	-405.80 to -381.60	0.79-1.21	-3.12 to 2.61	-1.02 to 1.27	2.52-3.99	64613-135098	-16 to -4
17 July	00h-08h	3.84-20.87	-424.30 to -386.60	0.87-1.92	-2.91 to 4.18	-1.69 to 1.18	2.81-5.56	49006-112269	-8 to 4
	08h-16h	22.49-44.84	-407.70 to -381.10	0.72-1.27	-2.24 to 3.69	-1.44 to 0.63	2.41-3.92	85088-133330	-8 to 2
	16h-24h	11.72-33.53	-381.70 to -355.60	0.68-1.09	-3.96 to 2.91	-1.07 to 1.42	2.43-4.03	21801-87259	-6 to 5
18 July	00h-08h	2.15-18.57	-357.80 to -325.20	0.42-0.92	-2.46 to 2.46	-0.86 to 0.81	1.95-3.68	16920-55202	-11 to -2
	08h-16h	18.76-37.95	-334.60 to -314.10	0.48-0.66	-2.46 to 1.57	-0.69 to 0.54	2.35-3.08	18704-53487	-10 to -4
	16h-24h	14.35-30.57	-328.30 to -316.20	0.56-0.70	-0.90 to 0.60	-0.21 to 0.28	2.62-3.45	23741-88624	-13 to -4
19 July	00h-08h	1.23-18.72	-341.20 to -301.20	0.62-0.82	-2.49 to 1.07	-0.36 to 0.67	2.83-4.24	17785-57816	-5 to -1
	08h-16h	19.00-35.42	-313.70 to -300.80	0.53-0.72	-3.11 to 1.19	-0.56 to 0.88	2.84-3.90	20321-48557	-6 to -2
	16h-24h	11.33-32.12	-304.80 to -289.40	0.56-0.88	-1.15 to 0.92	-0.43 to 0.32	3.06-4.97	11462-27958	-6 to 3
20 July	00h-08h	1.46-18.63	-296.60 to -278.00	0.74-1.43	-1.58 to 2.02	-0.66 to 0.33	4.35-8.76	8191-16061	0 to 6
	08h-16h	17.54-34.76	-292.10 to -284.60	0.85-2.10	-3.95 to 2.44	-0.54 to 0.99	5.15-12.31	9930-31671	-2 to 13
	16h-24h	10.82-30.71	-287.20 to -272.70	1.19-1.47	-3.40 to 1.79	-0.51 to 0.95	7.43-9.47	16821-33241	1 to 6
29 July	00h-08h	3.87-26.00	-372.10 to -332.40	0.98-1.96	-2.45 to 2.48	-0.62 to 0.62	4.06-7.78	22171-48825	-10 to -3
	08h-16h	26.76-50.41	-337.40 to -306.50	1.12-1.86	-3.29 to 4.10	-0.89 to 0.64	5.64-10.99	20560-40742	-5 to 4
	16h-24h	16.04-44.19	-338.60 to -303.10	1.26-2.32	-4.11 to 0.98	-1.31 to 0.96	4.04-8.02	19242-68459	-11 to 3
30 July	00h-08h	3.85-30.62	-331.80 to -313.80	0.83-1.48	-2.50 to 2.63	-0.59 to 1.39	4.00-5.77	26472-53451	-12 to -4
	08h-16h	31.57-57.10	-334.00 to -315.10	0.82-1.24	-2.85 to 3.57	-0.80 to 0.51	3.77-5.79	19493-48371	-14 to -6
	16h-24h	16.32-50.49	-315.20 to -334.70	0.75-1.24	-2.85 to 3.57	-1.22 to 0.85	3.77-5.79	19493-48371	-14 à -6

Correlation Analysis Between VTEC and Solar Parameters

To quantify the influence of minor solar wind fluctuations, Pearson, Spearman, and Kendall correlation coefficients were calculated between VTEC and solar parameters(V_x, B_z, E_y, D, P, T *and SYM-H)*. The analysis was conducted on two-time windows: Full Day (00h–24h) (**Appendix 3.a and 3.b)** and Night (19h–24h) **(Figures 8 and 9)**.

The results (presented as heatmaps) allow for a visual distinction of the relationships:

- **Nocturnal Phase (19h–24h):** Very strong correlations (often > 0.8) are observed. The parameters most strongly correlated with VTEC are solar wind speed (V_x), the B_z component, the electric field (E_y), and the SYM_H index.

- **Daytime (Full Day):** Correlations are generally weaker than at night. Temperature (T), speed (V_x), and proton flux (P) appear as the parameters most linked to VTEC during the day.

Figure 8 illustrates, from left to right, the **Pearson**, **Kendall**, and **Spearman** correlation coefficients computed during the nighttime phase for each investigated station in March.

Figure 9 presents the corresponding results for July. High color intensity (red for positive correlations and blue for negative correlations) reflects strong statistical relationships, whereas low color intensity indicates weak linear dependence.

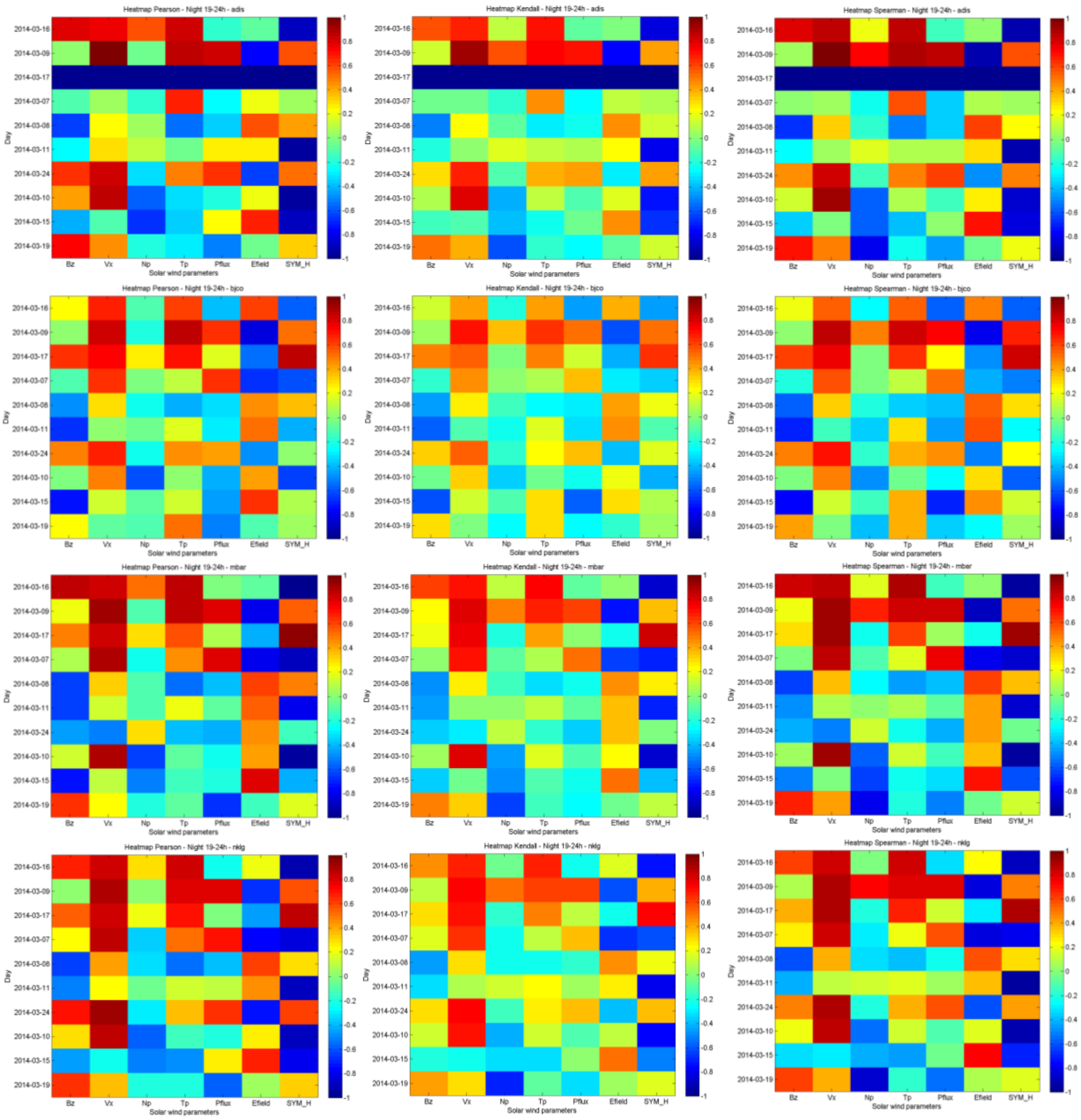

Figure 8: Correlation matrix (Pearson, Kendall, and Spearman) between VTEC and solar wind parameters (19:00–24:00 UT) during geomagnetically quiet days in March 2014.

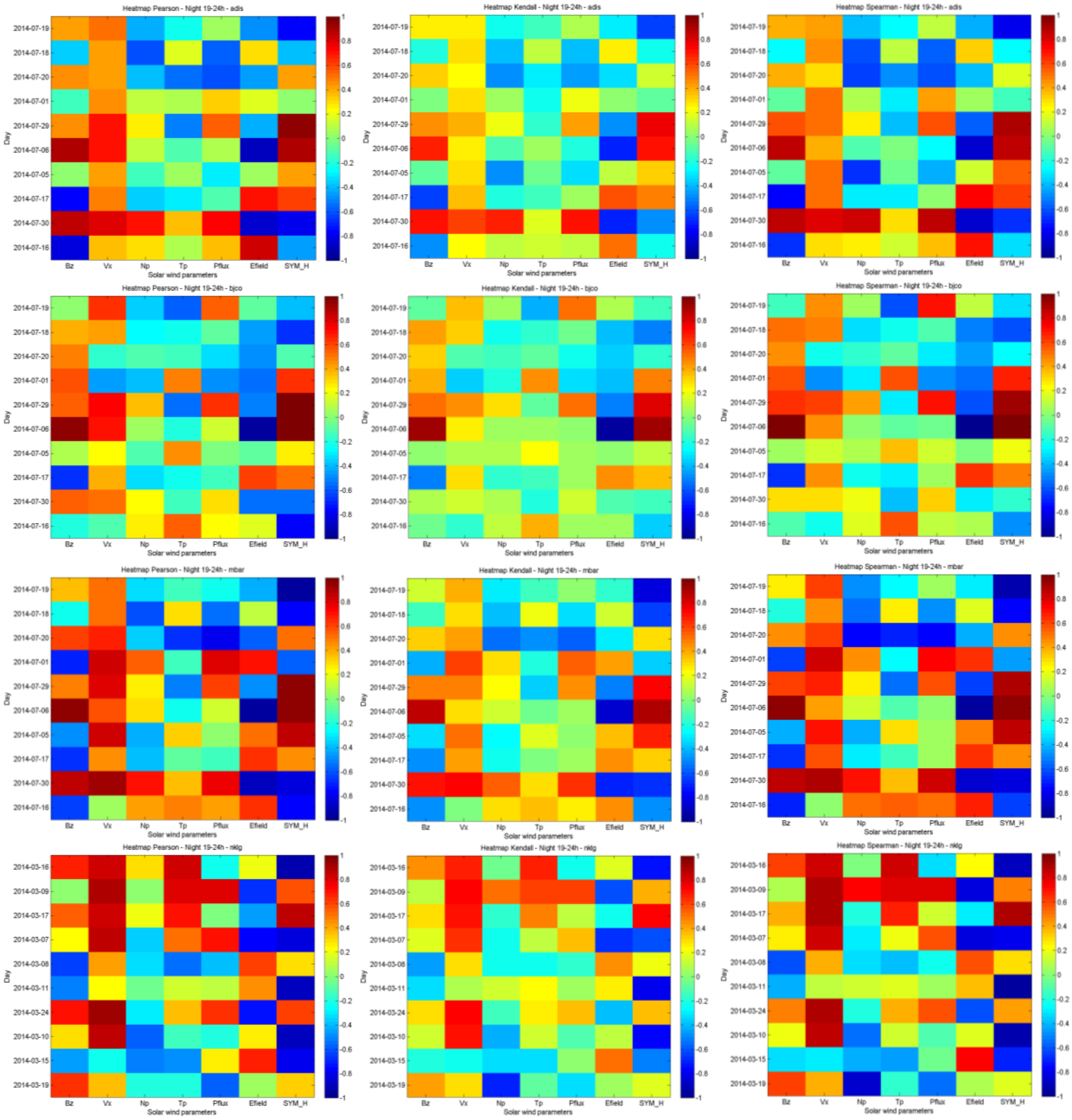

Figure 9: Matrice de corrélation (Pearson, Kendall, Spearman) entre VTEC et les paramètres du vent solaire (entre 19 et 24h) pour les jours calmes de juillet 2014.

DISCUSSION

The obtained results confirm that, even during geomagnetically quiet periods, minor fluctuations in the solar wind and interplanetary parameters induce significant variations in the Total Electron Content (TEC) over the African equatorial region.

The discussion proceeds from general TEC observations to an analysis of the influence of solar parameters on TEC and an estimation of their impact, based on correlation analyses (Pearson, Kendall, Spearman).

The observed diurnal TEC structure, characterized by a rapid rise after sunrise, a maximum around 12–16h UT, and a gradual decay in the evening, is consistent with the photo-ionization and electrodynamic redistribution processes described by Ayorinde and al.

(2016) [15]. However, the maximum amplitude varies from one station to another, highlighting the combined influence of longitude and proximity to the magnetic equator.

The main results reveal pronounced diurnal and seasonal TEC variability, with significantly higher values in March (80-110 TECU) than in July (40-60 TECU), which aligns with prior observations of the winter anomaly. The study also highlighted a longitudinal influence: the NKLG station (Gabon) systematically displays the highest TEC values, followed by ADIS (Ethiopia) and MBAR (Uganda), while BJCO (Benin) shows lower amplitudes. This reflects the influence of longitude and position relative to the magnetic equator on the Equatorial Ionization Anomaly (EIA) structure Bilitza and al. , (2019) [16] ; Falayi and al., (2023) [5].

Seasonally, our results show higher TEC in March (equinox) than in July (solstice), consistent with the observations of Huang and Cheng (1996) [17] and Karia and Pathak (2011) [18], who reported more pronounced ionization peaks during equinoxes than during solstices. This seasonal asymmetry can be explained by the increased efficiency of electrodynamic drifts and plasma redistribution during equinoxes Rastogi & Klobuchar, (1990) [19].

In July, solar wind density and pressure appear higher, but accompanied by lower speeds and moderate temperatures, whereas in March the opposite is observed, with faster, hotter winds at lower densities and pressures. This agrees with the work of Frédéric Ouattara and Christine Amory-Mazaudier (2009) [20], showing that solar wind proton density is greater when speed is lower. Pressure and density alone do not appear to have a direct impact on ionospheric activity.

Contrary to the idea proposed by Dinga and al. (2023) [12] that a TEC greater than 70 TECU would signal a magnetic perturbation, our results show that such values can occur during quiet days, particularly in March. This confirms the necessity of a multi-parameter approach combining geomagnetic indices (SYM-H), solar wind speed, and temperature, rather than relying solely on TEC values to classify ionospheric disturbances.

Globally, there is a very clear difference between daytime and nighttime correlations. Nighttime correlations (19-24h) are much stronger (often exceeding 0.8) than daytime correlations. This suggests that the physical processes linking the solar wind to the ionosphere are more direct or less noisy during the night in the absence of dominant photo-ionization. It indicates a more direct and less noisy coupling between the solar wind and the nighttime ionosphere, supporting the conclusions of Joshua and al. (2021) [3] and Koala and al. (2022) [4] on the increased sensitivity of the equatorial ionosphere to minor solar wind fluctuations during quiet periods.

During the day, temperature, speed, and proton flux are the parameters most closely linked to VTEC, whereas at night, solar wind speed, the interplanetary magnetic field's B_z component, the electric field, and the SYM_H index show much stronger correlations.

For full days, temperature emerges as the most correlated parameter regardless of the correlation type; this is certainly due to the strong radiation linked to insolation.

It should be noted that for the geomagnetically calmest days (the first five on the list for March), all stations show a strong nocturnal correlation with speed as well as temperature, unlike other days. However, for July, only speed presents this trend. Furthermore, despite local variations, general trends are quite similar across the different stations (ADIS, BJCO, MBAR, NKLG), all located in equatorial or low-latitude regions. This indicates that the observed phenomena are large-scale rather than merely local.

CONCLUSION AND PERSPECTIVES

This study highlighted the impact of minor solar wind fluctuations on ionospheric variability in Equatorial Africa, focusing on geomagnetically quiet days in March (equinox) and July (solstice) 2014. Through the analysis of four GNSS stations (ADIS, BJCO, MBAR, NKLG), this work confirms that even in the absence of major geomagnetic storms, ionospheric dynamics remain closely linked to interplanetary conditions.

It has been demonstrated that the diurnal TEC peak alone is not a sufficient indicator to qualify a day as quiet or disturbed, thus contradicting previous conclusions based solely on this threshold.

The most significant contribution of this study lies in the correlation analysis. A clear distinction has been established between diurnal and nocturnal regimes. During the day, TEC variability is strongly influenced by solar radiation, with solar wind temperature emerging as a predominantly correlated parameter. However, the strongest and most statistically significant correlations appear at night (19:00–24:00 UT). During this period, in the absence of direct photo-ionization, solar wind speed (V_x), the B_z component of the interplanetary magnetic field, the electric field E_y), and the $SYM - H$ index present much stronger correlations and become dominant factors, with correlation coefficients frequently exceeding 0.8.

Furthermore, this work complements existing research, often focused on geomagnetic storms, by demonstrating that subtle changes in solar parameters are sufficient to significantly modulate equatorial TEC. These results highlight the need for continuous monitoring and multi-parameter analysis to understand and model the ionosphere in such a complex and under-instrumented region as Africa.

However, this study presents certain limitations that point towards future perspectives, namely:

- he analysis period, although covering two contrasting seasons, is limited to a single year (2014) and a specific level of solar activity.
- The number of stations, while geographically distributed, remains insufficient to fully capture the longitudinal complexity of the region.

Based on the conclusions of this study, several avenues for future research can be proposed to deepen the understanding of Sun-Earth interactions in the African equatorial region:

1. **Study over a complete solar cycle:** Extend the analysis over a longer period covering different phases of solar activity (minimum, maximum, ascending, and descending phases). This would allow for verification of whether the correlation relationships identified during quiet periods (particularly the five quietest days of each month) persist or change with increasing solar activity.
2. **Investigation of nocturnal phenomena:** Deepen the study of strong nocturnal correlations to better understand coupling mechanisms. It would be pertinent to

analyse the link between solar parameters and the occurrence of specific phenomena, such as the development of Rayleigh-Taylor instability, plasma bubbles, and ionospheric scintillations that degrade GNSS signals.

3. **Inter-regional comparison:** Compare the ionospheric response of the African equatorial band with other equatorial regions (South America, Southeast Asia) to identify regional specificities and test model robustness.

4. **Data improvement:** Encourage the installation of new GNSS stations and the creation of open, continuous databases for the African region to reduce the current observational deficit and foster research.

REFERENCES

[1] E. A. Data (2025), “Variation of Total Electron Content over May 10–13, 2024 Geomagnetic Super Storm in South Africa,” Int. J. Astrophys. Space Sci., vol. 13, no. 2, pp. 21-35, Apr. 2025, doi: 10.11648/j.ijass.20251302.11.

[2] T. Ram, A. Bhaskar, S. Vemuri, H. Le, R. Hajra, and al., “Super-Intense Geomagnetic Storm on 10–11 May 2024: Possible Mechanisms and Impacts,” Space Weather, vol. 22, no. 8, 2024, doi: 10.1029/2024SW004XXX.

[3] B. W. Joshua, J. O. Adeniyi, C. Amory-Mazaudier, & S. J. Adebiyi (2021). On the pre-magnetic storm signatures in NmF_2 in some equatorial, low- and mid-latitude stations. Journal of Geophysical Research: Space Physics, 126(8), e2021JA029459.

[4] S. Koala, Y. Sawadogo, & J. L. Zerbo (2022). Solar wind and geomagnetic activity during two antagonist solar cycles: Comparative study between the solar cycles 23 and 24. International Journal of Physical Sciences, 17(3), 57–66.

[5] O. Falayi, A. O. Oyeyemi, & S. T. Oyedokun (2023). Analysis of Total Electron Content over the African low-latitude region during the maximum of Solar Cycle 24 (2012–2014). Journal of Atmospheric and Solar-Terrestrial Physics, 231, 105632.

[6] http://sopac.ucsd.edu

[7] ftp.aiub.unibe.ch/CODE/year

[8] https://celestrak.com/GPS/almanac/Yuma

[9] https://www.omniweb.gsfc.nasa.gov

[10] R. Warnant, (1996), étude du comportement du contenu électronique total et de ses irrégularités dans une région de latitude moyenne. Application aux calculs de positions relatives par GPS. Doctoral thesis from the Royal Observatory of Belgium.

[11] A. S. Muhammad, (2003) Contribution au positionnement en temps réel par GPS. Prédiction de la correction ionosphérique. Doctoral thesis from the University of Paris Observatory, P. 49-52.

[12] J.B. Dinga, O.P. Okolandzaud, J.F.P. Boungou Poaty et C. Bouka Biona, (2023). Estimated Impacts Induced by The Magnetic Activity Index (Dst) on the Local Total Electronic Content (TEC) in Africa Equatorial Zone; European Journal of Applied Sciences - Vol. 11, No. 3, P. 291-309.

[13] R. Fleury., (2017). Cours sur le "GPS : Ionosphere". Institut Mine-Télécom. Rabat.

[14] https://www.gfz-potsdam.de/en/kp-index/

[15] T.T. Ayorinde, A. B. Rabiu et C. Amory-Mazaudier, (2016). Inter-hourly variability of Total Electron Content during the quiet condition over Nigeria, within the Equatorial Ionization Anomaly region; Journal of Atmospheric and Solar-Terrestrial Physics ,145, P. 21-33.

[16] D.Bilitza, L.-A. McKinnell, B. W. Reinisch, and Fuller-Rowell, T. J. (2019). Characterization of the equatorial ionization anomaly in Africa during solar cycle 24. Journal of Geophysical Research: Space Physics, 124(7), 5432–5447

[17] Y-N. Huang et K. Cheng, (1996). Solar cycle variations of the equatorial ionospheric anomaly in total electron content in the Asian region; Journal of Geophysical Research, Vol 101, No. A11, P. 24513-24520.

[18] S. P. Karia et K. N. Pathak, (2011). GPS based TEC measurements for a period August 2008-December 2009 near the northern crest of Indian equatorial ionospheric anomaly region; J. Earth Syst. Sci. 120, No. 5, P. 851-858.

[19] R. G. Rastogi. and Klobuchar, J. A. (1990). Ionospheric electron content within the equatorial F2 layer anomaly belt. Journal of Geophysical Research: Space Physics, 95(A11), 19045–19052.

[20] Frédéric Ouattara et Christine Amory-Mazaudier (2009) Solar–geomagnetic activity and Aa indices toward a standard classification, Journal of Atmospheric and Solar-Terrestrial Physics 71, 1736–1748.

[21] J.L. Zerbo, F. Ouattara, C.A. Mazaudier, J.P. Legrand et J.D. Richardson, (2013). Solar Activity, Solar Wind and Geomagnetic Signatures; Atmospheric and Climate Sciences, 3, P. 610-617.

[22] A. Shimies, C. Amory-Mazaudier, R. Fleury, A. M. Mahrous et A. F. Hassan, (2014). Transient variations of vertical total electron content over some African stations from 2002 to 2012; Advances in Space Research, 54, P. 2159-2171.

[23] R. Steyaert and J. L. V. Eck, (2014). Les tempêtes solaires et leur impact sur les réseaux électriques.

[24] J. Lilensten and P. L. Blelly, (2000). Du Soleil à la Terre Collection Grenoble Sciences Dirigée par J. Bornarel, ouvrage publié avec le concours du ministère de l'éducation nationale, de la Recherche et de la Technologie. ISBN 2.86883.467.1. ED Sciences, http://www.spaceweather.com and http://www.solarmonitor.org

[25] P. Lassudrie-Duchensne et R. Fleury., (septembre 2012). Cours sur le "GPS. Ionosphère". Ecole de Brest.

[26] C. A. Smith., (1987), Ionospheric TEC Estimation with a singele-frequency GPS receiver. The effect of ionosphere on communication, navigation and surveillance system, Ionospheric effect symposium; Naval Reserch Laboratory 5-7 may, P. 145-150.

[27] S. Nahmani., (2012). Météorologie en traitement de données GPS pour les Sciences de l'environnement : contribution à l'étude de la Mousson en Afrique de l'Ouest. Doctoral thesis, Université Pierre et Marie Curie, Paris, P.24-25.

[28] G.K. Hartmann, R. Leitinger, (1984). Range Errors due to Ionospheric and Tropospheric Effects for signal frequencies above 100Mhz. Bulletin Géodésique, 58, P. 109-136.

[29] J. J. Spilker, (1978). GPS signal structure and performance characteritics. Navigation, Washington; The journal of the Institue of Navigation, Washington, Vol.25, N0 2, P. 121-146.

[30] H. Rishbeth (1971) Polarization fields produced by winds in the equatorial F-region Planetary and Space Science Volume 19, Issue 3, Pages 357-369.

APPENDIX 1: DIURNAL VARIABILITY OF VTEC ON QUIET DAYS IN MARCH (16, 17, 19, AND 24) AND JULY (19, 20, 29, AND 30) 2014 FOR THE FOUR STATIONS (ADIS, BJCO, MBAR, AND NKLG).

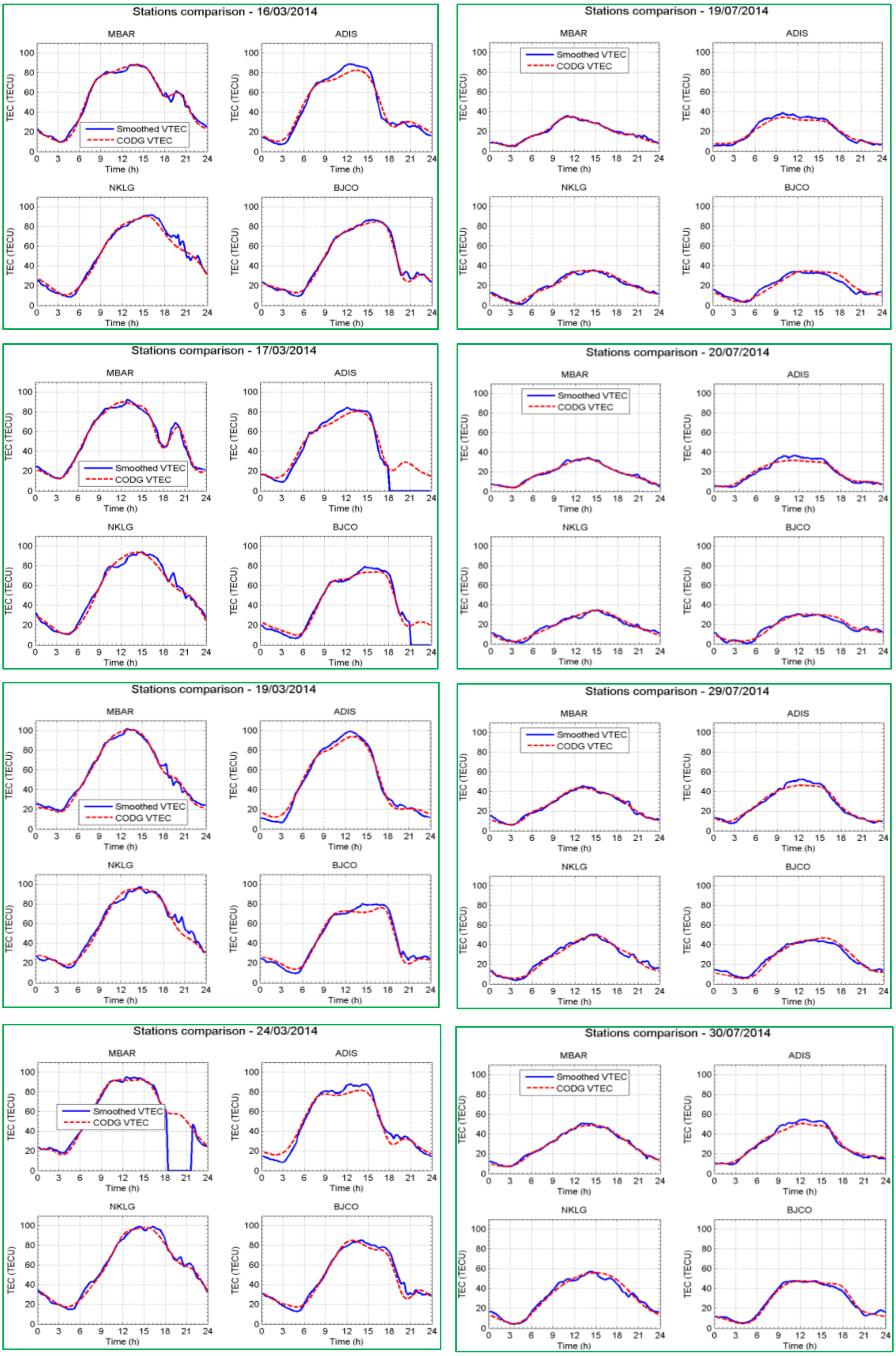

APPENDIX 2: EVOLUTION OF SOLAR WIND PARAMETERS (V_x, B_z, E_y, D,P, T ET SYM-H) DURING THE QUIET DAYS OF MARCH (15 AND 19) AND JULY (16 AND 30) 2014.

DOY 75

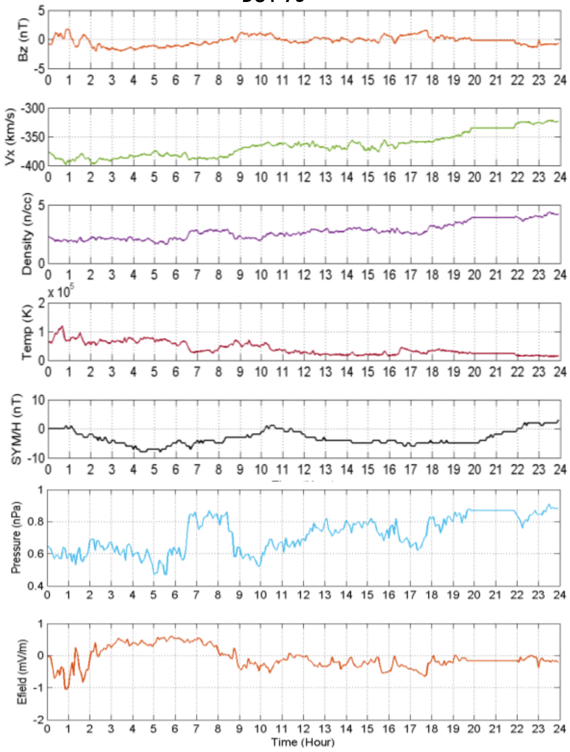

DOY

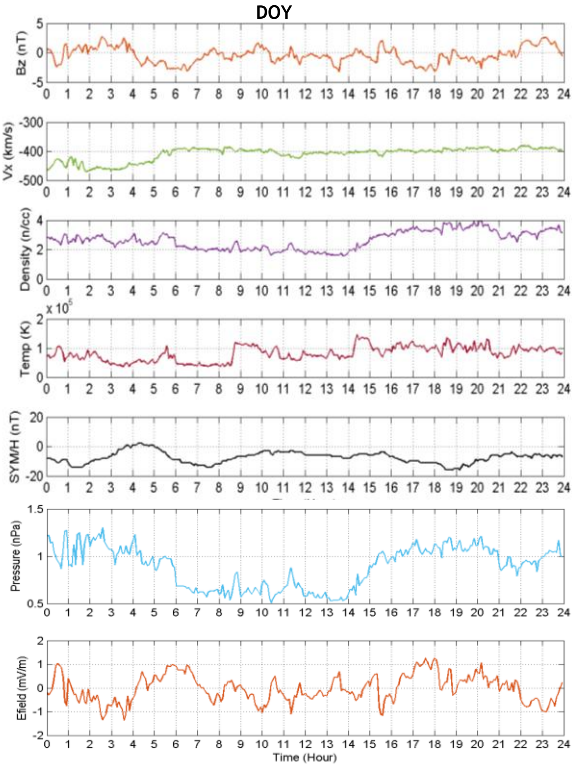

DOY 79

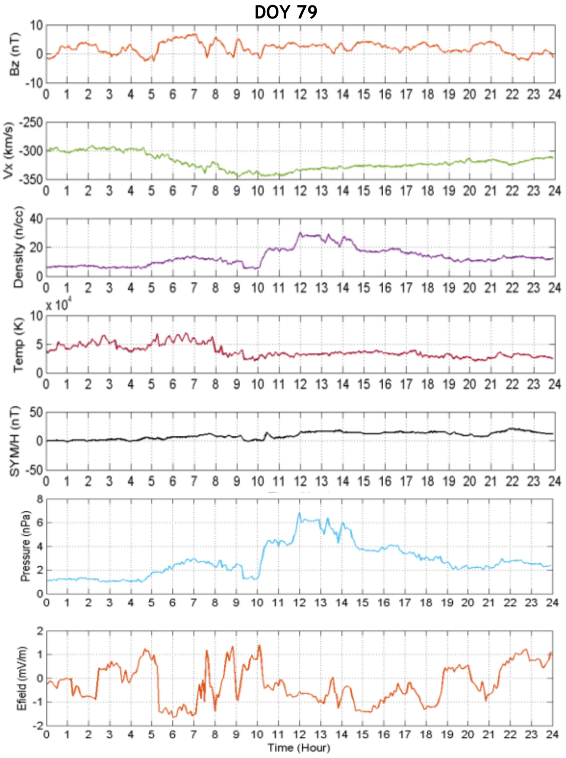

DOY

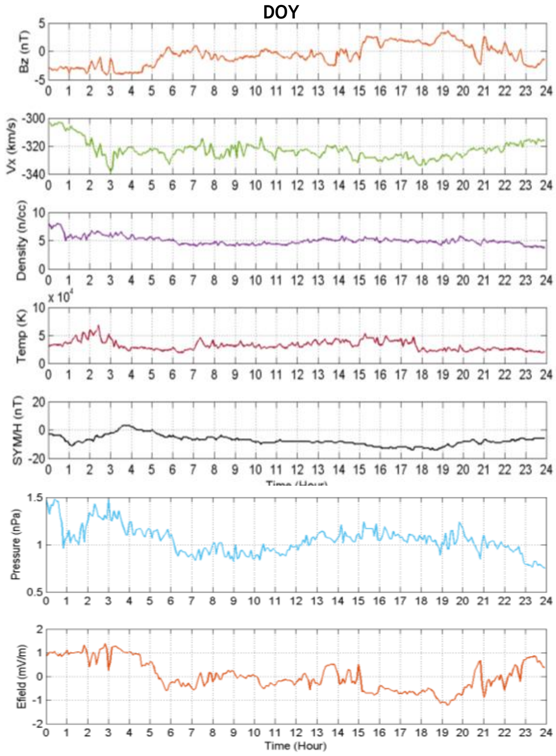

APPENDIX 3.A: CORRELATION MATRIX (PEARSON, KENDALL, SPEARMAN) BETWEEN VTEC AND SOLAR WIND PARAMETERS (ENTIRE DAY) FOR THE QUIET DAYS OF MARCH 2014.

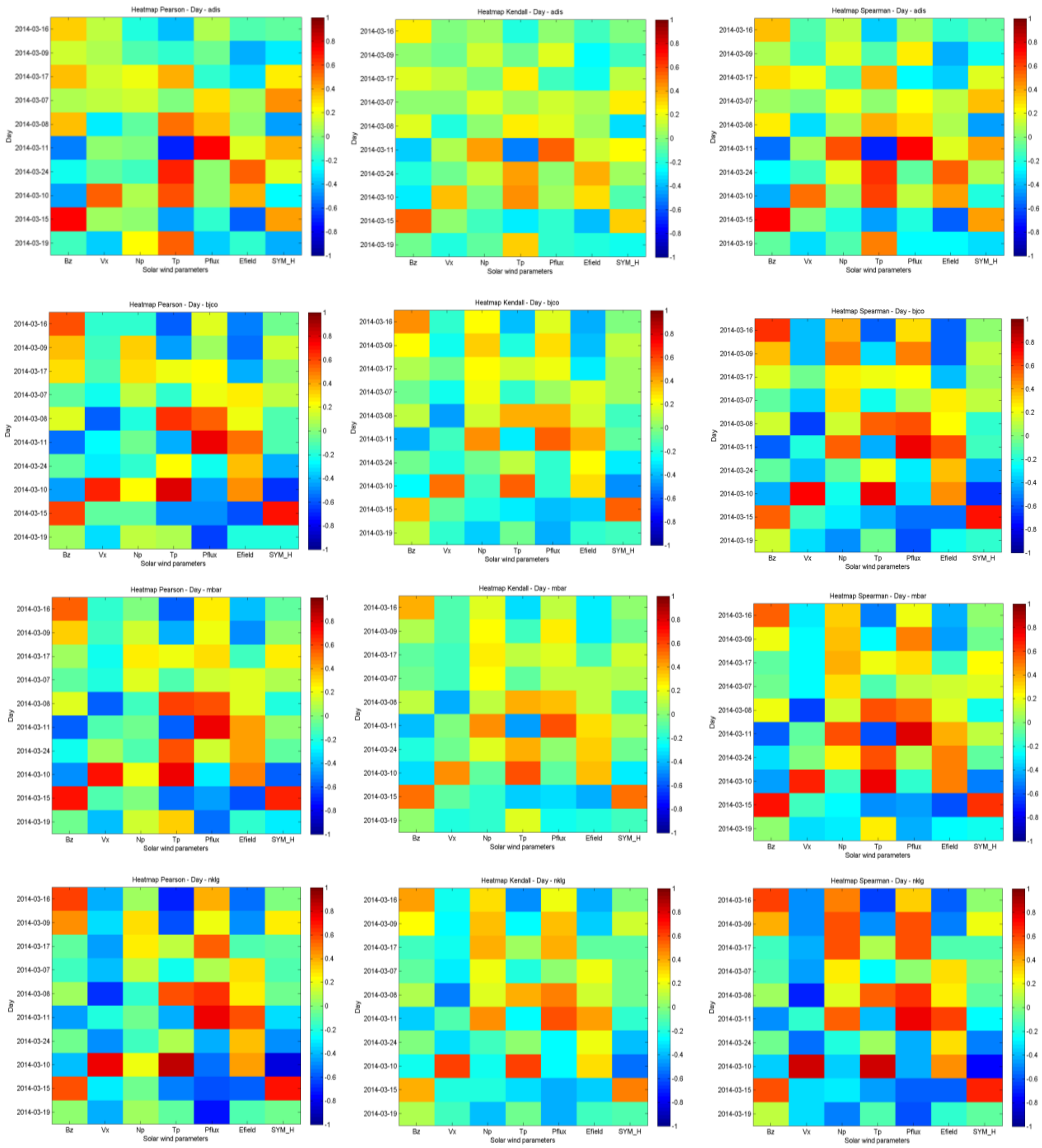

APPENDIX 3.B: CORRELATION MATRIX (PEARSON, KENDALL, SPEARMAN) BETWEEN VTEC AND SOLAR WIND PARAMETERS (ENTIRE DAY) FOR THE QUIET DAYS OF JULY 2014.

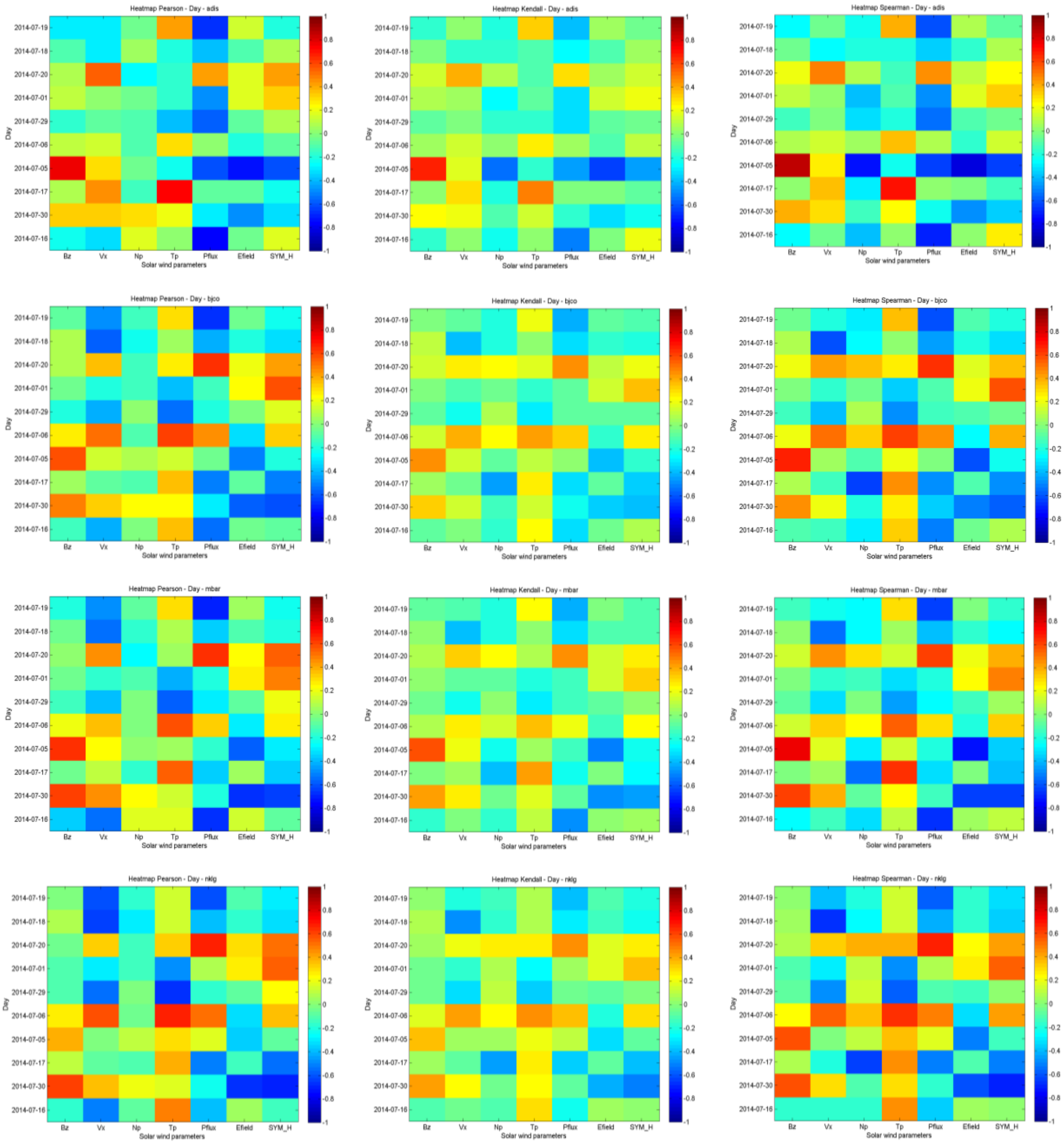

APPENDIX 4: EXCERPTS OF THE MATLAB ALGORITHM CODES USED FOR CALCULATIONS AND FOR PLOTTING CURVES AND HEATMAPS.

a. ***tec_notigs.m***

```
clear all;
clc;

%% A. read the file tec_igs.txt that contain some useful informations on the processing files
fidz=fopen('biais_resu.txt','w');
% in the same directory
for tour=1:1                                    % loop 0
  fide=fopen('tec_notigs.txt','r');
  if tour >= 2
    for ii=1:11*(tour-1)
      line=fgetl(fide);   % jump the good number of lines
    end
  end
line=fgetl(fide);                     % comment
name_gps=fgetl(fide);                 % name of station gps
line=fgetl(fide);
[A]=sscanf(line,'%f');
day_lu=A(1); month=A(2); year=A(3);   % date
path_rinex=fgetl(fide);               % path of the rinex file
path_comp=fgetl(fide);                % path for the files of Hatanaka
path_dcb=fgetl(fide);                 % path of the dcb file
path_yuma=fgetl(fide);                % path of the almanac file
path_ionex=fgetl(fide);               % path of the codg file
path_tmp=fgetl(fide);                 % path of the working
line=fgetl(fide);                     % maximum value of vtec to plt the results
fclose (fide);
clear A
% end of enter
plot_vtec_max=str2num(line);

%%%%%%%%%%%%%%%%%%%%%%%%%%%%%%%%%%%%
% if I want the 12 month in one pass
if month == 13
  m1=1 ;  m2=12;
  %if tour == 1, m1=6; end     %%%%%%%%%%%%%%%%%%%%%!!!!!!!!!!!!!!!!!
  else
  m1=month; m2=month;
end

%% B. for all days of the month
for loop_month=m1:m2                        % loop 1
month=loop_month;
if day_lu == 99
  n_day = day_month(month,year);  n1=1;
  else
  n1=day_lu; n_day=day_lu;
end
```

b. *vtec_jour_1mois.m*

```
sta_rinex='adis';                             %%% MARKER NAME %%%
year_beg=2011; year_end=2011;                 % year : begin and end
mois_deb=01;  mois_fin=12;                    % month : begin and end
ind_dst=0;       % =1 si on tracer l'indice magnétique Dst
dossier_dst='E:\les_mensuels\';         % folder of dst index
% end inputs

igs='n';   % prendre toujours n
fprintf('%s%s\n','vtec_jour_1mois.m : tracer des variations journalieres du VTEC sur 1 mois avec superposition de l''indice dst - station = ',sta_rinex)

for year=[year_beg:year_end]       % boucle 0 annee

  %input_tec=['d:\vtec_resu\'  sprintf('%04.4d',year) '\' sta_rinex '\'];    % dossier fichiers vTEC, dans la boucle si on veut tracer plusieurs annees
  input_tec=['E:'  sprintf('%04.4d',year) '\'];    % dossier fichiers vTEC, dans la boucle si on veut tracer plusieurs annees
  for month=mois_deb:mois_fin    % boucle 1 mois

    fprintf('%s%4.0f%s%5.0f\n','v_tec pour le mois = ',month,' annee = ',year)
    [day_begin,day_last]=bornes(month,year);
    fprintf('%s%5.0f%5.0f\n','quantieme entre = ',day_begin,day_last)
    plot_vtec(input_tec,year,month,sta_rinex,igs,day_begin,day_last,ind_dst,dossier_dst)       %vtec=f(jours)

  end    % fin for month
end   % fin for year

fclose ('all');
return
%
%-------------------------------------------------------------------------------
%
function plot_vtec(support,year,month,cgps,igs,day_begin,day_last,ind_dst,dossier_dst)
% tracer vTEC

for day=1:31
  tabx(1:96,day)=day;
end
taby=zeros(96,31);

r_init=day_begin;
kk=0;
for day=day_begin:day_last

  chaine=[support cgps sprintf('%03.3d',day) '0.txt'];
  fidr=fopen(chaine,'r');
  if fidr ~= -1
    %fprintf('%5.0f\n',day)
    line=fgetl(fidr);
    if igs == 'y'
      A = fscanf(fidr, '%f', [2 inf]);    % (time,vtec)
      elseif igs == 'n'
      A = fscanf(fidr, '%f', [3 inf]);    % (time,vtec,vtec ionex/codg)
    end
```

c. *tec_2d_tl.m*

```
clear all;
clc;

path_ini='E:\2015\annuel\data\';   % chemin des fichiers VTEC issus de tec_notigs.m
%path_ini='H:\trait_koud\trait_rinex\koud_vtec\';
sta_gps='CPVG';    % marker name: attention : il doit etre en majuscule
sta_gps=upper(sta_gps);
% j'ai repris le tableau de coordonnees de Omar sans verifier !
% secteur amerique
if sta_gps == 'AREG', lat=-16.47;  lon=-71.49; end
if sta_gps == 'BRAZ', lat=-15.95;  lon=-47.88+360;  end
if sta_gps == 'CKIS', lat=-21.2;   lon=-159.8; end
if sta_gps == 'GLPS', lat=-0.74;   lon= -90.3; end
if sta_gps == 'ISPA', lat=-27.12;  lon= -109.34; end
if sta_gps == 'MKEA', lat=19.8;    lon= -155.46; end
if sta_gps == 'RECF', lat=     -8.05; lon=     -34.95; end
if sta_gps == 'RIOP', lat=     -1.65; lon=     -78.65; end
if sta_gps == 'KOUR', lat=     5.25;  lon=     -52.51; end
% secteur Europe-Afrique
if sta_gps == 'ADIS', lat=     9.04;  lon=     38.77; end
if sta_gps == 'BJCO', lat=     6.3847;  lon=   2.45; end
if sta_gps == 'MAL2', lat=     -3.0;  lon=     40.19; end
if sta_gps == 'MOIU', lat=     0.29;  lon=     35.29; end
if sta_gps == 'NKLG', lat=     0.35;  lon=     9.67; end
if sta_gps == 'ULUB', lat=     -11.631;  lon=  27.485; end
if sta_gps == 'CPVG', lat=     16.732;  lon=   337.065; end
if sta_gps == 'DAKR', lat=14.7209;  lon=-17.4395+360; end
if sta_gps == 'NICO', lat=35.141;  lon=33.396 ; end
if sta_gps == 'DATG', lat=14.6762;  lon=360-17.4204 ; end
if sta_gps == 'ASCG', lat=-7.91628;  lon=360-14.33266 ; end
if sta_gps == 'KOUD', lat=12.253;  lon=-2.363+360 ; end
%if sta_gps == 'BECH', lat=     ±33; lon=      ±3; end   % station Algerie,coordonnee fausse
%if sta_gps == 'OGLA', lat=     ±29; lon=      ±7; end % station Algerie,coordonnee fausse
if sta_gps == 'TLSE', lat=43.561;  lon=1.481;  end
if sta_gps == 'MAS1', lat=27.7637;  lon=360-15.6333;  end
if sta_gps == 'BJPA', lat=11.10567;  lon=2.79375;  end
if sta_gps == 'RABT', lat=33.9981028;   lon=360-6.8542889; end
if sta_gps == 'OUCA', lat=31.207;       lon=352.133; end
if sta_gps  == 'MBAR', lat=-0.601;      lon=30.738; end
if sta_gps  == 'DJIG', lat=11.52629;    lon=42.8471; end
if sta_gps  == 'OUAG', lat=12.366;      lon=-1.53; end
if sta_gps  == 'LOM1', lat=12.356;      lon=358.487; end
if sta_gps  == 'LOM1', lat=12.356;      lon=358.487; end
if sta_gps  == 'NDJA', lat=12.128;      lon=15.034; end
if sta_gps  == 'YKRO', lat=6.871;       lon=354.760; end
```

d. ***solar_data_plot.m***

```
clear; clc;

%% --- 1. Chemin dossier contenant le fichier (modifiable ici) ---
folder_data = 'E:\Solar_data\solar_script';
filename_data = 'SolarW_2014.lst.txt';

folder_data = strrep(folder_data, '\', '/');
chemin_complet = fullfile(folder_data, filename_data);

if ~exist(chemin_complet, 'file')
    error(['File not found: ', chemin_complet]);
end

%% --- 2. Chemin dossier sauvegarde figures (modifiable ici) ---
folder_save = 'E:\Solar_data\solar_script\juillet\Result_1';
folder_save = strrep(folder_save, '\', '/');

if ~exist(folder_save, 'dir')
    mkdir(folder_save);
end

%% --- 3. Paramètres à tracer (1 = oui, 0 = non) ---
plot_Bz       = 0;  % Composante Bz
plot_Speed    = 1;  % Vitesse
plot_Vx       = 0;  % Vx Velocity
plot_Density = 0;  % Densité
plot_Temp     = 0;  % Température
plot_Pressure= 1;  % Pression
plot_Efield   = 1;  % Champ électrique
plot_SYMH     = 0;  % SYM/H

%% --- 4. Lecture du fichier ---
fid = fopen(chemin_complet, 'r');
if fid == -1, error('File cannot be opened.'); end

data = [];
while ~feof(fid)
    line = fgetl(fid);
    if ischar(line)
        valeurs = sscanf(line, '%f');
        if length(valeurs) == 12
            data = [data; valeurs'];
        end
    end
end
```

e. ***VTEC_Cor_Solarwind.m***

```
clear; clc;

%% === 1. Paramètres du fichier ===
folder_data = 'E:\Solar_data\solar_script\donnees_solaires\';
filename    = 'SolarW_2014.lst.txt';
file_path   = fullfile(folder_data, filename);

%% === 2. Définition du format de lecture ===
fmt = '%4d %4d %3d %3d %8.2f %8.1f %8.1f %7.2f %9f %6.2f %7.2f %6d';

%% === 3. Lecture du fichier ===
fid  = fopen(file_path, 'r');
data = textscan(fid, fmt, 'Delimiter','', 'MultipleDelimsAsOne', true);
fclose(fid);

%% === 4. Mise en table avec noms de colonnes ===
T = table(data{1}, data{2}, data{3}, data{4}, ...
          data{5}, data{6}, data{7}, data{8}, ...
          data{9}, data{10}, data{11}, data{12}, ...
    'VariableNames', {'Year','DOY','Hour','Minute','Bz','Speed','Vx','Density','Temp','Pressure','Ey','SYM_H'});

%% === 5. Suppression des valeurs aberrantes ===
aberrant_values = [999.9, 99999.9, 99999.9, 999.99, 9999999, 99.99, 999.99, 999.9];
params = {'Bz','Speed','Vx','Density','Temp','Pressure','Ey','SYM_H'};
for i = 1:length(params)
    T.(params{i})(T.(params{i}) == aberrant_values(i)) = NaN;
end

%% === 6. Construction du temps compatible MATLAB2014a ===
Year   = double(T.Year);
DOY    = double(T.DOY);
Hour   = double(T.Hour);
Minute = double(T.Minute);

T.Time = datenum(Year, 1, 1, Hour, Minute, 0) + (DOY - 1);

%% === 7. Entrée de la période par mois et jour ===
start_month = 1;  start_day = 1;
end_month   = 1;  end_day   = 2;

start_num = datenum(2014, start_month, start_day, 0, 0, 0);
end_num   = datenum(2014, end_month, end_day, 23, 59, 59);
```